DEUTSCHES ELEKTRONEN-SYNCHROTRON DESY

DESY 83-004
LAPP-TH 72
January 1983

CALCULATION OF THE GLUEBALL MASS SPECTRUM OF SU(2) AND SU(3) NON-ABELIAN LATTICE GAUGE THEORIES I: INTRODUCTION AND SU(2)

by

K. Ishikawa

City College, CUNY, New York

G. Schierholz

II. Institut für Theoretische Physik der Universität Hamburg

M. Teper

L.A.P.P., Annecy

ISSN 0418-9833

NOTKESTRASSE 85 · 2 HAMBURG 52

To be sure that your preprints are promptly included in the
HIGH ENERGY PHYSICS INDEX ,
send them to the following address (if possible by air mail) :

DESY
Bibliothek
Notkestrasse 85
2 Hamburg 52
Germany

DESY 83-004
LAPP-TH 72
January 1983

Calculation of the Glueball Mass Spectrum of SU(2) and SU(3) Non-Abelian Lattice Gauge Theories I: Introduction and SU(2)

K. Ishikawa
City College, CUNY, New York

G. Schierholz
II. Institut für Theoretische Physik der Universität Hamburg

M. Teper
L.A.P.P., Annecy

Abstract

We describe a direct method for calculating the glueball mass spectrum in QCD and apply it to the SU(2) non-abelian gauge theory. The method involves the application of Monte Carlo methods to the lattice regulated theory. We calculate the masses of states of various spins and parity. We check for the absence of finite size effects, for the desired renormalization group dependence and that our higher mass states do not merely reflect a continuum cut. Finally we repeat the calculation in the "Hamiltonian" limit and in the high temperature deconfining phase of QCD.

I. Introduction

Motivation

The present moment in particle physics is a particularly exciting one. The problem of understanding the strong interactions appears to be on the brink of resolution. To reach this point has required two developments: firstly the construction of a theoretically appealing and phenomenologically reasonable fundamental field theory, quantum chromodynamics (QCD), and secondly the development of non-perturbative methods, the lattice [1] Monte Carlo techniques [2,3], to solve and hence to give a real meaning to the QCD Lagrangian.

In this series of papers we shall discuss the calculation of that part of the hadron spectrum that is composed primarily of the gluon degrees of freedom. These hadrons, the glueballs, are of particular interest given the historical development of QCD. Quantum chromodynamics has its origins in the merger of two [4,5] rather separate areas of investigation: on the one hand hadron spectroscopy gave us quarks and the global symmetries of the theory, while on the other hand deep inelastic processes turned this into a non-abelian gauge theory by requiring asymptotic freedom. As a result of its local non-abelian character QCD possesses a richer spectrum than that of the traditional quark spectroscopy. In particular a whole sector of the spectrum should consist (before mixing) of pure glue states [4]. These glueball states are very much a prediction of QCD, and the absence of specific experimental information on these states provides us with the opportunity of making quantitative predictions that have no experimental bias.

Our calculation will be of the pure glueball spectrum before mixing with quarks. That is to say we shall perform the calculation in the pure non-abelian gauge theory. In most cases the effects of mixing may well be smaller than our quoted statistical errors. In particular this should be the case for those glueballs, the oddballs, which have quantum numbers inaccessible to a simple $q\bar{q}$ pair. The main advantage of doing a full calculation with fermions is that we could express the overall mass scale more readily in physical units (GeV). As it is we set our overall scale through the string tension [6] which is a less reliable procedure.

Preliminary results of our calculations have appeared in several brief publications over the last year, in particular results on the SU(2) [7] and SU(3) [8] glueball spectra, the renormalization group behaviour of the SU(2) spectrum [9] and on low-lying oddballs in SU(3) [10]. Here we will present some new results, and we will also take the opportunity to give a detailed account of our methods and of what we have learned during the course of our work.

In the present paper (I) we shall describe the general method and shall discuss its application to the SU(2) non-abelian gauge theory. Since corresponding calculations are about a factor of 10 slower for SU(3) than for SU(2), we have performed most of the checks, such as searching for renormalization group behaviour or finite size effects, in SU(2) rather than SU(3). The present paper describes all this. The companion paper [11] (II) will contain our results for the physically more interesting (but, as it turns out, not so different) SU(3) glueball spectrum. In our conclusion we shall compare our results to those of other recent calculations [12-22] of glueball masses.

Lattice gauge theory [1]

Our starting point is the Feynman path integral representation [23] of the gauge theory in Euclidean space time:

$$Z = \int [dA_\mu(x)]\, e^{-\frac{1}{2g^2}\int d^4x\, \mathrm{Tr}(F_{\mu\nu}F_{\mu\nu})} , \qquad (1)$$

where the field strength tensor is

$$F_{\mu\nu} = \partial_\mu A_\nu - \partial_\nu A_\mu + [A_\mu, A_\nu] . \qquad (2)$$

Note that the coupling has been absorbed into the matrix-valued vector field $A_\mu(x)$:

$$A_\mu(x) = g\, A^a_\mu(x)\, T^a , \qquad (3)$$

where the $A^a_\mu(x)$ are the gauge potentials and the T^a are a representation of the SU(2) or SU(3) Lie algebra.

As it stands the representation (1) is incomplete: any attempt at a calculation with (1) will encounter ultraviolet infinities. The conventional way to deal with this ultraviolet problem is to add to (1) a regularization prescription: the theory is first mutilated by the arbitrary removal of the offending high momentum/short distance components of the fields, and then these components are systematically reintroduced (in order of increasing momentum) while varying the coupling in such a way as to keep the theory finite - which means that beyond a certain momentum the reintroduction of the even higher momentum components will not affect the low energy physics. To implement the regularization procedure one must specify a momentum p_o such that momentum components higher than p_o are to be thrown away, and then the bare coupling g^2 in (1) is effectively the coupling on the size scale p_o^{-1}. We then take $p_o \to \infty$ varying $g^2(p_o)$ so as to keep the low energy ($p \ll p_o$) physics unchanged. The full speci-

fication of the theory is no longer scale invariant.

The widely applied regularization procedure in perturbative calculations is dimensional regularization [24]. Another way to remove high momenta is to remove small distances by discretising space-time [1]: if we put the theory onto a lattice of spacing a, we automatically restrict all the components of the momentum to be less than or equal to p_{max}, where

$$p_{max} = \frac{\pi}{a} . \tag{4}$$

To recover the full theory we let $a \to 0$. Once a is much less than the dynamical lengths in the theory, characterized by some correlation length ξ, the physics of the theory should remain unchanged as $a \to 0$ as long as we vary g^2 with a according to the usual renormalization group formula (which to two loops is the same for all regularization procedures, apart from the Λ parameter which can be related to, say, the more familiar Λ_{mom} via a perturbative calculation [32]). For reasons of calculational convenience we may also wish to confine space-time to a finite volume, say L lattice spacings in each direction. Then if

$$La \gg \xi \tag{5}$$

the physics should be the same as for the infinite volume limit.

The purpose of the above elementary discussion is to make the point that lattice QCD [25] is not some kind of qualitative approximation to "true" QCD: lattice QCD when treated in the appropriate region of parameters

$$La \gg \xi \gg a \tag{6}$$

is precisely "true" QCD.

We now turn to the detailed specification of the lattice regularized gauge

theory [1]. The basic geometric facets of the lattice are the sites, the links, the plaquettes, etc. If we had a scalar field we would place it on the sites (labelled by n):

$$\phi(x_\mu) \longrightarrow \phi(n) . \tag{7}$$

A vector gauge field belongs most naturally to the links joining neighbouring sites:

$$A_\mu(x) \to U_\mu(n) = e^{ia A_\mu} , \tag{8}$$

while a tensor field could naturally be associated with a plaquette. With fermions the situation is less straightforward, and this contributes to the difficulty in calculating with them.

So the degrees of freedom of our lattice system are the $N_c \times N_c$ unitary matrices $U_\mu(n)$ associated with the links of the lattice (N_c = number of colours). The partition function becomes

$$Z = \int \prod_n [dU_\mu(n)] \; e^{-S(U)} , \tag{9}$$

where the measure is the Haar invariant measure over the group. The action S(U) must reproduce the usual continuum Euclidean action in (1-3) in the limit $a \to 0$. An example is the Wilson action

$$S(U) = \beta \sum_n \left(1 - \frac{1}{N_c} \mathrm{Tr}\, \square\right) , \quad \beta = \frac{2N_c}{g^2} , \tag{10}$$

where Tr $\square$ means taking the trace of the matrix obtained by multiplying together the 4 matrices on the links forming the plaquette, and which we shall use in our work. In addition to having the correct continuum limit it also possesses positivity properties [26] that will be required in our calculations.

Monte Carlo solution

Formulated in Euclidean space-time, the lattice regulated gauge theory, as in (9), looks [25] just like a statistical mechanical system with a Boltzmann factor e^{-S}. This suggests [25] using methods developed for solving such systems. The method that interests us here is the Monte Carlo technique [2,3]. The essence of this method is the generation of gauge field configurations over the lattice according to the distribution $\prod_n [dU_\mu(n)]\, e^{-S(U)}$. Suppose we have generated N such configurations

$$\{ U_\mu(n) \}_{i = 1, \ldots, N} \quad . \tag{11}$$

Then any vacuum expectation value is given by

$$\langle \phi(U) \rangle \simeq \frac{1}{N} \sum_{i=1}^{N} \phi(\{U_\mu(n)\}_i) \quad , \tag{12}$$

where the approximate equality in (12) becomes exact as $N \to \infty$, and where the deviation from the correct value for finite N is $O(1/\sqrt{N})$. One may think of the gauge field configurations in (11) as representing typical "snapshots" of the vacuum, so that the vacuum expectation value of any functional ϕ may be obtained by averaging the values it obtains in these snapshots.

To obtain the SU(2) gauge field configurations we have used standard heat bath routines [27] and have followed the standard convention of sweeping through the lattice in a regular systematic fashion. For our SU(3) calculation (described in the companion paper (II)) we have performed some of our calculations sweeping regularly through the lattice, but the bulk of our calculations have been performed by picking at random the link to be updated [3]. We have also investigated the effects of using different random number generators. The results of this investigation, showing significant effects for some states, are described in

detail in ref. (11).

Calculating the mass spectrum

A general way to estimate the lowest glueball mass in the theory is to introduce some disturbance into the system and to observe the way the effects of this disturbance are damped at large distances away from the source of the disturbance: the damping will be exponential in distance (at large enough distances), and the scale of the exponent will be the lowest glueball mass. The disturbance could be a defect in the lattice, a change of boundary conditions (or size of the lattice), a local heating of the lattice, etc. Or, more conventionally, one can look at the long distance behaviour of a correlation function of some operator ϕ (which is local in time)

$$\langle \phi(t)\, \phi(0) \rangle \underset{t \to \infty}{\sim} e^{-\mu t} \quad , \tag{13}$$

where μ is the mass of the lowest mass glueball that communicates with (and so has the same quantum numbers as) the operator ϕ. By considering operators of various spins, parities and charge conjugations, J^{PC}, one can obtain the corresponding spectrum of glueball masses.

The problem with this method is that the mass determination can only be made where (13) is valid, and that is where the signal has become (exponentially) small. It is clear that a method such as the above is hardly the most appropriate for a Monte Carlo calculation. What we really want is a method where the mass is most reliably extracted where the signal is largest.

The transcription of the usual variational calculation onto the lattice is

such a method and was suggested by Wilson [28]. Suppose we have a system characterized by H and we want the ground state energy. The variational method instructs us to choose some à priori reasonable class of wave functions, $\{\phi\}$, and then to vary the wavefunction within this class so as to minimise the energy expectation value

$$\delta \left\{ \frac{\langle \phi^+ H \phi \rangle}{\langle \phi^+ \phi \rangle} \right\} = 0 . \tag{14}$$

Suppose $\tilde{\phi}$ is the wavefunction for which the minimum is achieved, and suppose $\tilde{E}$ is the corresponding energy. Then $\tilde{\phi}$ and $\tilde{E}$ are our best approximations to the true ground state wavefunction ϕ_o and energy E_o. Moreover, we know that

$$E_o \leqslant \tilde{E} . \tag{15}$$

On the lattice the relevant operator is not H but rather the transfer matrix [25] $V = e^{-Ha}$ (the Euclidean time translation operator). So the variational method will instruct us to search for a ϕ that maximises the expectation value

$$\delta \left\{ \frac{\langle \phi^+ e^{-Ha} \phi \rangle}{\langle \phi^+ \phi \rangle} \right\} = 0 \tag{16}$$

(since minimising H implies maximising e^{-Ha}). This is just what we wanted: a technique which involves searching for a large rather than a small signal.

The method can be extended to a general correlation function as follows (we represent the vacuum by $|\Omega\rangle$, and the complete sets of states we insert are energy eigenstates):

$$\frac{\langle \phi(t)\, \phi(0) \rangle}{\langle \phi(0)\, \phi(0) \rangle} = \frac{\langle \phi(0)\, e^{-Ht} \phi(0) \rangle}{\langle \phi(0)\, \phi(0) \rangle}$$

$$= \sum_{n=0}^{\infty} e^{-E_n t} \frac{|\langle \Omega | \phi | n \rangle|^2}{\sum_{n=0}^{\infty} |\langle \Omega | \phi | n \rangle|^2} \tag{17}$$

$$\leqslant e^{-E_o t}$$

so that (taking the E_n to be in order of increasing energy)

$$E_o \leqslant \frac{1}{t} \ln \frac{\langle \phi(0)\, \phi(0) \rangle}{\langle \phi(t)\, \phi(0) \rangle} , \tag{18}$$

and given some set of trial wavefunctions $\{\phi\}$, our best estimate for E_o will be

$$E_o = \frac{1}{t} \min_{\{\phi\}} \left[\ln \frac{\langle \phi(0)\, \phi(0) \rangle}{\langle \phi(t)\, \phi(0) \rangle} \right] . \tag{19}$$

Before continuing some comments are in order. First it is easy to see from (17) why at large enough t we recover (13). It is also clear that the more the operator ϕ projects onto the lowest energy state $|n=0\rangle$, i.e. the greater is $|\langle \Omega | \phi | n=0 \rangle|^2$, the sooner will the simple exponential behaviour (13) set in, and the larger will be the measured signal. Indeed in the limit where our operator ϕ projects entirely onto $|n=0\rangle$, we only need to measure the correlation function over one time lattice spacing because (19) will be exact for all t.

In practice one must work with a limited class of trial wave-functionals, $\{\phi\}$,

and then it is not clear how good the energy estimate using (19) really is except that we know that it provides an upper bound, as in (17). One test is to evaluate (19) for several values of t and check if E_0 is roughly independent of t. In practice one gets reasonably accurate measurements for $t = 0, a, 2a$, but beyond that the signal is largely lost in noise. If we define for our future convenience

$$\Gamma_t \equiv \langle \phi(t)\,\phi(0) \rangle \,, \tag{20}$$

then our variational calculational will be successful if we obtain

$$\frac{\Gamma_{2a}}{\Gamma_0} \approx \left(\frac{\Gamma_a}{\Gamma_0}\right)^2 . \tag{21}$$

We return now to our main goal, that is to calculate the lowest glueball masses for various J^{PC} quantum numbers. So first we form wave-functionals with the desired J^{PC} quantum numbers (see below), localised in some sense about the lattice sites. Then, since we are interested in masses, we form translationally invariant, zero momentum operators by simply summing up our basic operator over all spatial sites at a given time. We then ensure that our operator has no projection on the vacuum by explicitly subtracting the vacuum expectation value, this being only necessary for our 0^{++} operators. Equ. (19) then becomes

$$m(J^{PC}) = \frac{1}{t} \min_{\{\phi(J^{PC},\vec{p}=0)\}} \left[\ln \frac{\langle \phi(0)\,\phi(0) \rangle}{\langle \phi(t)\,\phi(0) \rangle} \right] . \tag{22}$$

We have not yet been very specific about the operators ϕ. Since the theory is

confining [2,6], the glueballs are colour singlets, and an (over)complete set of colour singlet operators is given by the set of all closed loops. By a loop we mean multiplying, in order, the U matrices along the links forming the perimeter of the loop:

$\phi = \phi(\mathrm{Tr}$ 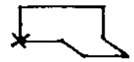 $)$. (23)

For ϕ to project strongly onto the lowest glueball state it should in some way mimic the structure of the glueball wavefunction. In the ideal calculation deep in the continuum limit, where the glueball is many lattice spacings across, the number of possible loops will be large, and in order for the computer time not to grow similarly, some way, aided by intuition, will need to be developed to select good wave-functionals, ϕ. In this paper we shall be content to work on as coarse a lattice as possible, while still being consistent with being in the continuum limit. In practice this means that the glueball will be about two lattice spacings across. So the typical loop contributing to ϕ will have an extension of two lattice spacings. Not surprisingly it is easy to find wave-functionals that project reasonably strongly ($\simeq$50 %) onto the lowest glueball state. However, even in this case the number of possible loops is extremely large, and a devoted variational calculational aiming at something like 100 % projection onto the lowest glueball state promises to be very lengthy.

Given this fact we pursue the following strategy [7]. We observe from the expansion (17) that even if our wavefunction possesses only, say, 50 % projection onto the lowest glueball state, the estimate

$$m = \frac{1}{a} \ln\left(\frac{\Gamma_a}{\Gamma_{2a}}\right) \tag{24}$$

can be very good even though $\ln(\Gamma_0/\Gamma_a)$ may be a poor estimate. This follows because the higher mass contributions to Γ_a and Γ_{2a} will be severely suppressed

by the exponential factors. To see how this works in practice we perform a simple illustration using numbers that are reasonable for our 0^+ calculation. We take the wavefunction to project equally onto two states. The first has a mass ma = 1 (this is the mass we want to measure), and then there is a higher mass excited state with Ma = 4. We insert these numbers into (17) to obtain Γ_a/Γ_o and Γ_{2a}/Γ_a, and then we insert the resulting values into (22) and (24). We find ma = 1.64 when we use (22) with t = a, ma = 1.35 when we use (22) with t = 2a, and ma = 1.05 when we use (24). Within the typical ($\simeq$10 %) statistical errors of such a calculation this last value is identical to the correct value ma = 1.

In the following work we shall search for several reasonably good wavefunctions and shall calculate Γ_{2a}/Γ_a for each of these wavefunctions, finally obtaining the glueball mass by statistically averaging the mass estimates obtained using (24) for each case:

$$ma = \frac{1}{N} \sum_{i=1}^{N} \ln \left[\frac{\Gamma_a}{\Gamma_{2a}} (\phi_i) \right] . \qquad (25)$$

Some comments. Clearly $\Gamma_{2a} \ll \Gamma_a$ and so to obtain Γ_{2a}/Γ_a to a given accuracy will require many more configurations than to obtain Γ_a/Γ_o to the same accuracy. In our example above it would be a factor of 10. We can gain a large part of this factor back by calculating with several wavefunctions at once, since in practice the computer time needed for generating a new gauge field configuration is much greater than the time needed to measure Γ_a and Γ_{2a} for a given wavefunction. All this is only true in our type of calculation, where the glueball is

about two lattice spacings across. Much deeper into the continuum limit the time for the measurement of Γ_a and Γ_{2a} will certainly dominate the total calculational time, and we anticipate that it will become much more difficult to find a "reasonably good" wavefunction. Here a dedicated variational calculation will need to be implemented cleverly if it is not to require astronomical amounts of time. In any case the variational calculation has the added advantage of yielding the glueball's detailed wavefunction as well as its mass.

At the heart of our calculation is the unitarity style decomposition in (17). The validity of (17) requires the lattice theory to possess appropriate positivity properties [25,26]. This is not automatic, and one reason we use the Wilson action with periodic boundary conditions is that it is known to possess these. One could argue that any action which has the correct continuum limit can be used, since deep in the continuum limit we will necessarily recover the correct positivity properties (along with full rotational invariance etc.). This is true, but in our calculation, where we work near the "edge" of the continuum limit, we judge it prudent to avoid such arguments.

Wavefunctions and angular momentum

We now describe how to construct operators of a given spin, parity and charge conjugation, J^{PC}. Charge conjugation reverses the direction of going around a loop. So the real part of the trace has C = +1, and the imaginary part has C = -1. In SU(2) the trace is real, and charge conjugation is trivial: hence we shall suppress that quantum number in our SU(2) calculations. It will reappear explicitly in our SU(3) calculations described in the companion paper (II). Parity inverts a spatial loop. Taking linear combinations of a loop and its parity inverse allows us to construct operators of P = +1 and P = -1. In particular

if our basic loop has a geometrical handedness, so that under inversion it becomes a loop which cannot be obtained from the original loop by any combination of rotations and/or charge conjugation, then we can use it to form operators of P = +1 and P = −1 for various J and C. Explicit examples will arise when we discuss our SU(2) calculation in this paper.

Angular momentum on the lattice is a little more subtle. Naively a cubic lattice is invariant not under the full rotational group but only under the 24 element octahedral group, one of the 32 standard crystallographic point groups. Indeed in the strong coupling limit one should use this group to classify the states of the system. In the continuum limit, however, one recovers full rotational symmetry, and the cubic character of the lattice only shows up on the scale of the cut-off, a. This recovery of full rotational symmetry is a dynamical phenomenon: the correlation length becomes large compared to the lattice spacing, so that on the size scale of the interesting "low energy" physics one can to an increasing (as $a \to 0$) accuracy disregard the particular granularity of space-time.

Because we are calculating properties of the theory in the continuum limit, we shall use the language of the full rotation group. On the other hand, because we are in fact working with a rather coarse lattice, we shall in practice be using only those rotations that are elements of the octahedral group. This means that we shall only be able to discuss glueballs of small J, and we shall not be able to form pure angular momentum states.

As an example we will now construct J = 0 and J = 2 operators (other examples will appear later in the paper). We pick as our angular momentum quantization axis one of the three axes of the cube, and we label the component of angular

momentum along this axis by m. We construct operators of a particular J, m by adding a basic loop to rotations of the same loop, with the coefficients of the terms in the sum being determined by the values of the appropriate rotation matrices. So, turning to J = 0 first, we choose as our basic operator the square loop, two links on a side, centred at the site n (Fig. 1a). We add to it, with coefficients +1, the two other such loops that can be obtained by rotations about n (Fig. 1b). The resulting operator will have a general decomposition

$$\phi = \sum_{J,m} \alpha_{Jm} \, \phi(J,m) \, . \tag{26}$$

We now rotate it by an angle ψ about the quantization axis,

$$\phi \to \phi' = \sum_{J,m} \alpha_{Jm} \, e^{-im\psi} \, \phi(J,m) \, . \tag{27}$$

For $\psi = \pi/2$, $\phi' = \phi$ by construction, so that in the above sum

$$m = 0, \; 4, \; 8, \; \ldots \tag{28}$$

Now rotate ϕ by an angle θ around one of the other axes

$$\phi \to \phi' = \sum_{J,m} \alpha_{Jm} \sum_{m'} d^{J}_{m'm}(\theta) \, \phi(J,m') \, . \tag{29}$$

If we focus on terms with $J < 4$, then (28) tells us m = m' = 0. Now ϕ is invariant under $\theta = \pi$ and $\theta = \pi/2$, whereas

$$d^{J}_{00}(\pi) = (-1)^{J} \, , \quad d^{J}_{00}\left(\tfrac{\pi}{2}\right) = 2^{-J} \sum_{n=0}^{J} (-1)^{n} \frac{(J!)^{2}}{((J-n)!\, n!)^{2}} \, . \tag{30}$$

So we see that only J = 0 contributes. Hence the operator we have constructed has J = 0 with an admixture of $J \geq 4$. We assume that the lightest glueball has J = 0 rather than $J \geq 4$, so we shall refer to such an operator as having J = 0.

To construct a J = 2 operator take our basic square in Fig. 1a and subtract from it the same loop but rotated by $\pi/2$ about the quantization axis (Fig. 1c). Applying (27) we find now that, because $\phi' = -\phi$, we have

$$m = 2, 6, \ldots \tag{31}$$

so that a J = 0 component is excluded. Rotating by π about one of the other axes we recover ϕ, i.e. $\phi \to \phi' = \phi$, whereas

$$d^J_{22}(\pi) = (-1)^{J-2} , \tag{32}$$

which tells us there is no J = 3 piece (equ. (31) already excluded J = 1). Hence this wave-functional has J = 2, 4, ... pieces. Assuming again that amongst all these the J = 2 glueball is the lightest, we shall refer to this operator as a J = 2 operator.

To construct $\vec{p} = 0$ wavefunctions of J = 0 or 2 we simply sum the above constructed wavefunctions over all lattice sites n (at a fixed time).

Momentum-smeared wavefunctions

Since we are interested in masses, the appropriate wave-functionals to use are ones with zero momentum. Occasionally we shall also use $\vec{p} \neq 0$ wave-functionals. The reason for this is as follows.

Consider working on a lattice with spatial extent $L_s a$ and temporal extent $L_t a$. On a given gauge field configuration we get one $\vec{p} = 0$ wavefunction (of any given type) at any given time, and hence we get altogether L_t measurements contributing to a correlation function such as Γ_{2a}. On the other hand the statistical error will decrease as $N^{-1/2}$, where N is the total number of measurements. At the same time the computer time required to generate a gauge field configuration

increases as the volume of the lattice, $L_s^3 L_t$. Thus the computing time required to achieve a given signal/error ratio will increase as L_s^3, if we vary L_s.

This means that in a calculation with $\vec{p} = 0$ wavefunctions one must keep L_s as small as possible. This is unfortunate because one would really like to reduce any systematic errors associated with finite size effects by making L_s as large as possible. Moreover, as we go deeper into the continuum limit, we must increase L_s even if we only demand that

$$L_s a > 2 R_G , \tag{33}$$

where R_G is the glueball size (this is surely the very least that one should require from a lattice with periodic boundary conditions). Hence from these purely practical considerations it is clear that we must do better.

A solution to this problem would be to use wave-functionals not just with $\vec{p} = 0$, but with any $\vec{p}$ small compared to the mass of the state being considered: $\vec{p}^2 \ll m^2$. For such a low momentum we expect the continuum dispersion relation, $E^2 = m^2 + \vec{p}^2$, to be valid, so m can be obtained from the correlation functions of such a $\vec{p} \neq 0$ wave-functional through an extension of (24):

$$m^2 = \left[\frac{1}{a} \ln\left(\frac{\Gamma_a}{\Gamma_{2a}}\right)\right]^2 - \vec{p}^2 . \tag{34}$$

For a lattice of spatial extent $L_s a$ the number of such low momentum states, and hence of possible measurements, increases as L_s^3, so that we lose nothing in going to larger lattices (to the extent that the various measurements are indeed statistically independent).

In a systematic calculation along these lines one would construct wavefunctions

of all possible momenta

$$p_x, p_y, p_z = \frac{2\pi n}{L_s}\ \frac{1}{a}\ ,\quad n = 0, 1, \ldots, \frac{L_s}{2}\ , \tag{35}$$

measure the corresponding energy of the glueball state

$$E = \frac{1}{a}\ \ln\left[\frac{\Gamma_a(\vec{p})}{\Gamma_{2a}(\vec{p})}\right] \tag{36}$$

and hence determine both the dispersion relation and the mass of the glueball (one could also take the opportunity to check for rotational symmetry in obvious ways).

One can also formulate this idea in position space rather than in momentum space. Instead of the $\vec{p} = 0$ wave-functional, which is given by the translationally invariant sum

$$\phi(\vec{p}=0, t) = \sum_{\vec{x}}\ \phi(\vec{x}, t)\ , \tag{37}$$

this then leads us to consider forming wave-functionals that are only partially translation invariant

$$\phi(\delta\vec{p}, t) = \sum_{\vec{x}\in D}\ \phi(\vec{x}, t)\ , \tag{38}$$

where D is some subset of the complete set of sites at time t, and where $\delta\vec{p}$ represents the spread of momenta contributing to ϕ. The simplest example is where D consists of just one site so that our momentum smeared wave-functional is just $\phi(\vec{x}, t)$. A more complicated example would be for D to be a 2^3 sublattice of neighbouring sites. The number of measurements will now vary as $(L_s/2)^3$. It is clear that the smaller is D (and hence the larger the number of measurements one can make), the greater will be the momentum smearing and the less reliable will be the extraction of the mass.

In some of our published work and in some of the calculations to be described later in this paper we have employed the position-space version of the above idea and have obtained results, which would have taken an order of magnitude more computing time if we had confined ourselves to $\vec{p} = 0$ wave-functionals.

We finish this section with a caveat concerning the construction of wavefunctions with a particular J and with $\vec{p} \neq 0$. Consider for example the J = 2 operator in Fig. 1c. Now consider the operator in Fig. 2 obtained by separating the two squares and duplicating them about the origin so that our overall wave-functional, which we consider centred at $\vec{x} = 0$, becomes

$$\Phi(\vec{o}, t) = \phi(\vec{x}, t) + \phi(-\vec{x}, t) - \mathcal{R}\phi(\vec{y}, t) - \mathcal{R}\phi(-\vec{y}, t)\ . \tag{39}$$

Here ϕ is the elementary 2x2 square as shown in the figure, and $\mathcal{R}\phi$ is the rotation of this square by $\pi/2$ as shown. $\vec{x}^2 = \vec{y}^2$ so that Φ has explicitly a negative sign when rotated by $\pi/2$ about the $\hat{z}$ axis. Hence it appears to be a J = 2 wave-functional. On the other hand if we consider a typical correlation function

$$\Gamma_t = \langle \Phi(\vec{o}, t)\ \Phi(\vec{o}, 0)\rangle\ , \tag{40}$$

the only place the negative sign in (39) enters (and it is this negative sign that makes J = 2 rather than J = 0) is in cross products, which themselves vanish as $|\vec{x} - \vec{y}|$ grows:

$$\langle \phi(\vec{x}, t)\, \mathcal{R}\phi(\vec{y}, 0)\rangle \xrightarrow[|\vec{x}-\vec{y}|\to\infty]{} e^{-\mu|\vec{x}-\vec{y}|}\ , \tag{41}$$

where μ is the J = 0 glueball mass. Hence for t large but smaller than $|\vec{x} - \vec{y}|$

$$\Gamma_t \sim e^{-\mu t} \tag{42}$$

(with the mass μ as above) despite the fact that Φ is a J = 2 operator. If we take $t \gg |\vec{x} - \vec{y}|$ (which we should), (42) remains correct except that some

extra inverse powers of t appear.

So we seem to have the asymptotic decay of the correlation function of a spin 2 operator being governed by a spin 0 mass! Actually what has happened is that we have constructed a state consisting of a J = 0 glueball with L = 2 relative to our lattice, hence also the extra powers of t in (42) as $t \to \infty$.

This example shows that one has to be careful in forming linear combinations of loops to simulate some spin J. If different pieces are even a little separated, this will show up in the correlation function at large enough t.

Systematic errors

As we have already pointed out, working with $\vec{p} = 0$ wave-functionals presses us to work with lattices that have as few spatial sites as possible. That means we do not work deep in the continuum limit, as specified by (6), but on lattices that are rather small and rather coarse. So we must check that our results do not change as we make a smaller (i.e. we check for the renormalization group behaviour of our mass estimates). We must also check that our results do not change as we increase the overall size of the lattice (i.e. we check for the absence of significant finite size effects).

Particularly important is the temporal extent of the lattice, since the physical temperature of the system is equal to the inverse of its temporal extent (for periodic boundary conditions). At high temperature non-abelian gauge theories are not confining. The deconfining phase transition for SU(2) and SU(3) gauge theories is at around 200 MeV [29]. Hence it is important to have $L_t a$ large enough for the lattice to be in the confined phase. Making L_t large enough does

not cost any extra time, since the number of measurements will be proportional to L_t. The physical temperature at which we shall work will typically be about 100 MeV. We shall present results for a range of temperatures and shall check for variations in our mass estimates. We shall also demonstrate what happens when we do the same calculation in the high temperature, deconfining phase of the theory.

Systematic errors can also arise in more subtle ways from the Monte Carlo procedure itself. One worry concerns the lack of true randomness of so-called random number generators [30]: does their use perhaps give rise to long range fluctuations? We shall go no further here than to mention this possible problem. A detailed analysis with a comparison of various random number generators will appear in the following SU(3) paper.

Another worry is that our generated gauge field configurations may get effectively stuck in some metastable state, so that our calculated masses are characteristic of this false vacuum and not the true vacuum. A procedure to deal with this is to generate 10 or 20 independent sequences of gauge field configurations rather than just one. One can generate such a sequence by starting with, say, unit matrices on all the links ($\beta = \infty$), then running at a randomly chosen value of β for, say, 20 configurations, and only then beginning to run at the desired value of β. Any "metastable states" should show up in comparing the results obtained from the different sequences of configurations. In the SU(2) calculations described in this paper we use 2 or 3 such sequences starting at $\beta = \infty$ (unit matrices) and $\beta = 0$ (random matrices). In the SU(3) calculations [8] we used about 10. We see no signal for any such "metastable states".

At a more practical level systematic errors can arise in our mass estimates

because of higher mass states contributing significantly to Γ_a. One can check this by comparing the measured values of Γ_a/Γ_o and Γ_{2a}/Γ_a. If we assume the lowest mass state to dominate both Γ_a and Γ_{2a}, then the ratio of Γ_a/Γ_o to Γ_{2a}/Γ_a obviously is just the probability for our wave-functional to project onto the lowest state. If this is $\gtrsim 40$ % or greater, then the higher mass admixture will be small. If, however, it is much less, then we have cause for concern. We shall perform such checks in the second part of this paper.

Once we have obtained our results for the various glueball masses in terms of a^{-1}, we shall want to reexpress these numbers in physical GeV units. The first step is to express a^{-1} in terms of a Λ mass scale through the usual renormalization group formula for $g^2(a)$ [31]. This Λ mass scale appropriate to the lattice action we are using can be expressed in terms of the more familiar Λ_{mom} through a perturbative calculation [32]. In principle we could now take Λ_{mom} from deep inelastic data. But unfortunately we do not know Λ_{mom} to better than a factor of two. The usual procedure therefore is to invoke the string tension, K [2,6]. This can be calculated on the lattice from the area decay of large Wilson loops [1]. One then uses the "experimental" value of the string tension given by

$$K = \frac{1}{2\pi\alpha'} \ (GeV)^2 , \qquad (43)$$

where α' is the slope of Regge trajectories (so $\alpha' \approx 0.9$). The argument for (43) is not particularly rigorous. Indeed open decay channels and fermion loops are not included properly. Nonetheless as a mass scale it is far more reliable than Λ_{mom}. In our work we shall express masses in GeV units by using (43). This introduces an unquantified systematic error. Our calculated mass ratios on the other hand are free of any such error.

The string tension is useful because it is a quantity that to "leading order" does not depend on fermions. There are other quantities in the pure gluon theory able to play a similar role. One is the gluon condensate, $\beta^{-1}\langle F^a_{\mu\nu} F^a_{\mu\nu}\rangle$, which is estimated in applications of QCD sum rules [33], and which can also be measured on the lattice [34]. Another is the fluctuation of the topological charge, $\langle [\sum_n F\tilde{F}(n)]^2 \rangle$, which can be related to the η' mass from arguments concerning the $SU(N_c)$ theory as $N_c \to \infty$ [35], or from effective Lagrangians [36] embodying similar physics. At the moment the status of the lattice calculations [37] of this quantity is obscure.

The ideal way to set the overall scale would be either for the experimentalists to come with an observed glueball, so that we could then tell where to look for the other glueballs, or for us to put in fermions, calculate the ρ meson mass, and use that as our scale. We expect progress in both directions in the not too distant future (and indeed two glueball candidates have recently been announced [38]).

Before leaving our discussion of systematic errors we should mention what is perhaps the most obvious one. In generating our lattice gauge field configurations we start from some readily constructed configuration, which will usually be totally atypical of the configurations at the value of g at which we wish to work. However, the Monte Carlo procedure is guaranteed to eventually produce us configurations which are in equilibrium with the desired e^{-S} Boltzmann factor, irrespective of the starting point. The problem is to know when this point has been reached. One way of telling is to measure such simple quantities as the action and to multiply by a "safety factor" of, say, 10 . So in our calculations the number of iterations before measurement will always be at least several

hundred, and frequently several thousand. In addition we check and compare results from different sequences of measurements. We believe that this type of systematic error contributes insignificantly to our results.

Statistical errors

To understand the statistical errors afflicting measurements of $\vec{p} = 0$ correlation functions, such as $\langle \phi(t)\,\phi(0)\rangle$, it is useful to write out this expectation value explicitly in terms of the way it is measured. Let $\phi(i\,;\vec{x},t)$ be the measured value on the gauge field configuration labelled by i of a glueball wave-functional centred on the point $(\vec{x},t)$. The $\vec{p} = 0$ wave-functional measurement is obtained by summing over the L_s^3 spatial sites labelled by $\vec{x}$

$$\phi(i\,;\vec{p}=0,t) = \frac{1}{L_s^{3/2}} \sum_{\vec{x}} \phi(i\,;\vec{x},t) \,. \qquad (44)$$

The $\vec{p} = 0$ correlation function $\langle \phi(t)\,\phi(0)\rangle$ is then obtained as follows:

$$\langle \phi(t)\,\phi(0)\rangle = \frac{1}{N} \sum_{i=1}^{N} \frac{1}{L_t} \sum_{t'=1}^{L_t} \frac{1}{L_s^3} \Big\{ \sum_{\vec{x}} \phi(i\,;\vec{x},t'+t) \Big\} \qquad (45)$$

$$\cdot \Big\{ \sum_{\vec{y}} \phi(i\,;\vec{y},t') \Big\} \,.$$

The objects in the curly brackets are just the $\vec{p} = 0$ wavefunctions. The first sum represents the average of the measurements over all N gauge field configurations. The sum over t' uses time translation invariance

$$\langle \phi(t)\,\phi(0)\rangle = \langle \phi(t'+t)\,\phi(t')\rangle \qquad (46)$$

to boost the number of measurements. One may further boost the number of measurements in special cases. For example if $L_s = L_t$, then we can obtain 4 sets of measurements from a given configuration by defining the time axis

to point in each of the 4 possible directions.

The individual ϕ in (45) will fluctuate about some mean value that will depend on β. These fluctuations will be uncorrelated in all the terms of the product in (45), except for those terms very close together. There are $(L_s^3)^2$ such terms, so the net fluctuation in the product will be proportional to $\sqrt{(L_s^3)^2} = L_s^3$. The signal on the other hand comes from those terms close enough to have an appreciable correlation, i.e. $\vec{x} \approx \vec{y}$, and there are $O(L_s^3)$ such terms.

If we label $\langle \phi(t)\phi(0)\rangle$ by a subscript N denoting the total number of configurations used, so that $\langle \phi(t)\,\phi(0)\rangle_\infty$ is the exact value, then (45) gives us

$$\langle \phi(t)\,\phi(0)\rangle_N = \langle \phi(t)\phi(0)\rangle_\infty \pm \sigma \sqrt{\frac{\xi_t}{L_t}} \sqrt{\frac{\xi_c}{N}} \,, \qquad (47)$$

where the second term is the statistical error. The factor of $\sqrt{L_t N}$ in (47) is just what one expects from $L_t N$ uncorrelated measurements. However, our measurements are not totally uncorrelated. There will be some correlation between measurements at neighbouring times in a given configuration, and also some correlation between gauge field configurations that are close in the generated sequence of configurations. These correlations are represented by the effective correlations lengths ξ_t and ξ_c in (47).

In most of our calculations the correlation function is small even over one lattice spacing, hence we expect $\xi_t \simeq 1$. For the magnitude of ξ_c we have no expectation. Our experience with measuring glueball correlation functions is that generally ξ_c is not very large.

To illustrate ξ_c we have measured it for the average action in a configuration

(i.e. the plaquette expectation value). Let $A(i)$ be the plaquette expectation value for the i'th lattice configuration (in the sequence in which they were generated). Split the total number of configurations, N , into K blocks of M sequential configurations and consider the subaverages

$$\bar{A}_j = \frac{1}{M} \sum_{k=1}^{M} A\left((j-1)M+k\right) . \tag{48}$$

Let the KM values of $A(i)$ have a standard deviation $\sigma(A)$, and let the K values of $\bar{A}_j$ have a standard deviation of $\sigma(\bar{A})$. Then

$$\sigma(\bar{A}) = \frac{\sigma(A)}{\sqrt{M/\xi_c}} . \tag{49}$$

We have performed such an exercise on an 8^4 lattice at β = 2.2, 2.3, 2.4 with 2400, 1850 and 950 configurations, respectively. We used M = 25 and also M = 30 to check for the stability. The configurations came in two sequences: in one case the original starting configuration was random (corresponding to $\beta = 0$), and in the other case all links were taken to be unit matrices (corresponding to $\beta = \infty$). The results for ξ_c are plotted in Fig. 3. We observe that ξ_c is surprisingly large. Whether such a long "correlation length" is peculiar to measurements of the action is something we do not know. We also note some indication of a systematic difference between the sequence starting from $\beta = 0$ and the sequence starting from $\beta = \infty$. The quality of this data, however, is not good enough for any firm conclusion on this point.

Let us return now to (47). We use the notation Γ_t for the correlation function. We now claim that σ is calculable so that (47) can be written

$$(\Gamma_t)_n = (\Gamma_t)_\infty \pm \frac{\Gamma_0}{\sqrt{n}} \tag{50}$$

as long as

$$\Gamma_t \ll \Gamma_0 \quad \text{and} \quad \langle \phi \rangle = 0 , \tag{51}$$

where n is the number of uncorrelated measurements; so for example in (47)

$$n = L_t N / \xi_t \xi_c . \tag{52}$$

[Proof: the measurement of $(\Gamma_t)_n$ involves n measurements of the random variable $y = \phi(t)\phi(0)$. The distribution of y has a mean

$$\langle y \rangle = \langle \phi(t)\phi(0) \rangle \underset{\Gamma_t \ll \Gamma_0}{\approx} \langle \phi(0) \rangle^2 \underset{\langle\phi\rangle = 0}{=} 0 \tag{53}$$

and a width

$$\begin{aligned} \sigma^2 = \langle y^2 \rangle - \langle y \rangle^2 &\approx \langle y^2 \rangle \\ &= \langle [\phi(t)\,\phi(0)]^2 \rangle \\ &= \langle [\phi(t)]^2 [\phi(0)]^2 \rangle \\ &\underset{\Gamma_t \ll \Gamma_0}{\approx} \langle [\phi(t)]^2 \rangle \langle [\phi(0)]^2 \rangle \\ &= \Gamma_0^2 , \end{aligned} \tag{54}$$

which gives us (50) as desired .]

In most of our calculations (51) will be satisfied and (50) will be valid. The quantities we shall usually measure are Γ_a/Γ_0 and Γ_{2a}/Γ_a . Using (50) we find

$$\left(\frac{\Gamma_a}{\Gamma_0}\right)_n = \left(\frac{\Gamma_a}{\Gamma_0}\right)_\infty \pm \frac{1}{\sqrt{n}} \tag{55}$$

and

$$\left(\frac{\Gamma_{2a}}{\Gamma_a}\right)_n = \left(\frac{\Gamma_{2a}}{\Gamma_a}\right)_\infty \pm \frac{(\Gamma_a/\Gamma_0)^{-1}}{\sqrt{n}} . \tag{56}$$

In practice equations (55) and (56) are very important. It is clear from (55) that a rough estimate of Γ_a/Γ_0 can be obtained very rapidly. Typically measure-

ments on about 100 configurations will suffice. From the fluctuations in Γ_a/Γ_0 we can estimate n, i.e. the overall correlation length in our measurements. We now can estimate, from (56), the error which our measurement of Γ_{2a}/Γ_a will possess after any number of configurations. Equ. (56) highlights the desirability of using as good a wavefunction as possible. Maximising Γ_a/Γ_0 minimises the eventual statistical error on Γ_{2a}/Γ_a, which via (24) will be the source of our mass estimate.

Now that we understand the error on Γ_{2a}/Γ_a, how does this translate into an error for the mass

$$m = \frac{1}{a} \ln \left(\frac{\Gamma_a}{\Gamma_{2a}} \right) \quad ? \tag{57}$$

Let the mass m have (asymmetric) errors $+\delta m_+$ and $-\delta m_-$. Using (57) we find

$$\delta m_{\mp} = \mp \frac{1}{a} \ln \left[1 \mp \left(\frac{\Gamma_0}{\Gamma_{2a}} \right) \frac{1}{\sqrt{n}} \right] , \tag{58}$$

while it is clear that asymptotically

$$\delta m_{\mp} \underset{n \to \infty}{\approx} \frac{1}{\sqrt{n}} \frac{1}{a} \left(\frac{\Gamma_0}{\Gamma_{2a}} \right) . \tag{59}$$

It is also clear that this behaviour will only set in once $a\,\delta m$ is small. In particular while δm_- behaves roughly like $1/\sqrt{n}$ from fairly early on, this is not the case for δm_+, which has a highly irregular behaviour, being ∞ until a certain value of n, n_0 say, at which point it collapses very rapidly with increasing n. In Fig. 4 we plot the factor by which δm_+ decreases when the number of measurements is doubled. Note that we <u>always</u> do better than the $1/\sqrt{n}$ expectation once $n > n_0$. On the basis of the $1/\sqrt{n}$ factor in (50) one is tempted to say that if there is no signal after measurements on, say, 10000

configurations, then doubling the number of configurations will not buy you much. Fig. 4 shows that this is not true: either it will not buy you anything at all (δm_+ stays at ∞), or the error will be dramatically reduced!

The second point to note is that while Γ_{2a}/Γ_a will have a normal probability distribution, the mass estimate m will not. Thus when we quote a mass as being $m \pm \delta m_{\pm}$, the reader should be aware that the two standard deviation limit on the mass is <u>not</u> $m \pm 2\delta m_{\pm}$. Generally we will provide the reader with the values of Γ_{2a}/Γ_a, so he can make his own estimates. A problem only arises once the error in Γ_{2a}/Γ_a is not small, and in that case the problem will be with δm_+ and not with δm_-. We note that in this case Γ_a/Γ_0 will provide a definite upper bound for the mass, which will make any concern about the true extent of the 2σ effect irrelevant.

The above analysis of statistical errors also has implications for what is the best way to do a dedicated variational calculation, where we vary ϕ so as to maximise Γ_a/Γ_0. Let us parameterise Γ_a/Γ_0 by the lowest mass, m, contribution which we are interested in, plus an effective higher mass, M, piece:

$$\frac{\Gamma_a}{\Gamma_0} = \alpha\, e^{-m a_t} + (1-\alpha)\, e^{-M a_t} , \tag{60}$$

where we allow for the possibility that the temporal and spatial lattice spacings differ, $a_t \neq a_s$. The point of the variational calculation is to maximise α. Now, an increase in α may be masked by the statistical error, and this will be worst in the limit of large a_t where the $e^{-m a_t}$ factor will be very small, or, less obviously, in the limit of small a_t where

$$\delta \left(\frac{\Gamma_a}{\Gamma_0} \right) = \delta\alpha \left(e^{-m a_t} - e^{-M a_t} \right) \tag{61}$$

$$\approx \delta\alpha\, (M-m)\, a_t \underset{a_t \to 0}{\longrightarrow} 0 .$$

The best value of a_t to use is the one for which the ratio of $\delta(\Gamma_a/\Gamma_0)$ to the error is as large as possible for a change $\delta\alpha$ in α. As we have seen, the error will be roughly independent of a_t, so we want

$$\frac{\delta\left(\frac{\Gamma_a}{\Gamma_0}\right)}{\delta\alpha} = 0 \ , \tag{62}$$

which is satisfied by

$$a_t = \frac{1}{M-m} \ln \frac{M}{m} \ . \tag{63}$$

So for a dedicated variational calculation this is the best temporal lattice spacing to use.

We shall later find that for the 0^+ glueball, $M \approx 4m$ typically, and for the 2^+ glueball typically $M \approx 2m$. So (63) becomes

$$a_t \approx \begin{cases} \frac{0.5}{m(0^+)} & : 0^+ \\ \frac{0.7}{m(2^+)} & : 2^+ \end{cases} \tag{64}$$

Now, as we are pressed to work with lattices of minimal spatial extent, we must keep a_s as large as possible (consistent with being in the continuum limit), and this requirement will clash with (64). In practice

$$a_s \approx 1.2/m(0^+) \approx 2.4/m(2^+) \tag{65}$$

in our calculations. This emphasises the desirability of using lattices with $a_t < a_s$. A second observation is that a variational calculation tuned to work best for one glueball is not necessarily going to be optimised for a glueball of different mass.

A final caveat is this. Generally we will have some basic wavefunctions ϕ_i, and we search for the linear combination $\phi = \sum_i \alpha_i \phi_i$, which will maximise Γ_a/Γ_0. Given finite errors on all the $\langle \phi_i \phi_j \rangle$ products in Γ, one must take care that the maximisation procedure does not merely search for the linear combination where fluctuations are maximal, so that Γ_a/Γ_0 sits on such an upward fluctuation! One should not consider a wave-functional better if the increase of Γ_a/Γ_0 over its largest value with the ϕ_i is not much larger than the statistical error. This caveat is especially relevant if one uses Γ_{2a}/Γ_a for a variational calculation.

11. The SU(2) Calculation

We will base our calculation upon the Wilson action [1] (10) as has been mentioned. For this action we have for sufficiently small coupling constants

$$a = \frac{57.5}{\Lambda_{mom}} e^{-\frac{3\pi^2}{11}\beta} \left(\frac{6\pi^2}{11}\beta\right)^{\frac{51}{121}} , \tag{66}$$

where we have expressed the lattice Λ parameter in terms of Λ_{mom} [32]. We shall assume that in our region of couplings ($\beta \gtrsim 2.2$) a is reliably given by (66). This is on the basis of previous work by other authors [6,39]. Note also that rotational symmetry has been restored [40] at these values of β which is related.

We shall use periodic boundary conditions. This is <u>crucial</u> to being able to use very small lattices: with periodic boundary conditions the conditions on our lattice are translation invariant. With other boundary conditions the boundary will usually be a special place, and its effects will pollute the physics two or three lattice spacings inward. This is illustrated in Fig. 5, where we show

the results of antiperiodic boundary conditions:

$$U_\mu(n+e_\nu L_{s,t}) = U_\mu^+(n) \quad , \quad e_\nu \text{ unit vector in } \nu\text{'th direction.} \tag{67}$$

We plot the average action of the sublattice obtained from a 10^4 lattice by systematically stripping layers of sites in all directions inwards from the boundary (leaving an L^4 lattice embedded at the centre of the 10^4 lattice). The dashed line is the average value of the action on an 8^4 lattice, at $\beta = 2.3$, with periodic boundary conditions. In Tab. 1 we present values of the average action as measured on lattices of various sizes with the boundary conditions (67). It is clear that in order to work with $\vec{p} = 0$ wave-functionals under such boundary conditions one would have to go to enormously large lattices.

Choosing the lattice and lattice parameters

Let a_s, a_t be the spatial and temporal lattice spacings of our $L_s^3 L_t$ lattice and let R_G be the diameter of the glueball. In order for the calculation of glueball properties to be credible, we require

$$\min\left(\frac{L_t a_t}{2}, \frac{L_s a_s}{2}\right) \gg R_G \gg \max(a_t, a_s) \tag{68}$$

and

$$T\ (=\text{temperature}) = \frac{1}{L_t a_t} \ll 200\ \text{MeV} \quad , \tag{69}$$

so that the lattice is not too coarse, not too small and not too hot.

A priori we do not know R_G, and the first part of the calculation involves obtaining an estimate for it. To do so we calculated Γ_a/Γ_0 for 0^+ wavefunctions composed of planar loops of various sizes ranging from 1 x 1 to 3 x 3 on a 6^4 lattice at $\beta = 2.3$ (for now take $a_s = a_t \equiv a$). The value of Γ_a/Γ_0 peaked for the 1 x 2 and 2 x 2 loops, see Fig. 6, indicating that

$$R_G \approx (1.5 - 2.0) \cdot a(\beta = 2.3) \tag{70}$$

For a more sophisticated analysis supporting (1) we refer to ref. (41).

In Fig. 7 we plot the lattice spacing, a, half the spatial lattice extent, $\frac{1}{2} L_s a$, and the glueball size, R_G, as functions of β. The scale is in fermi, using (66) and measurements of the string tension [6]. The curves are for $L_s = 4$ and 8.

From Fig. 7 it is clear that if one wants to have L_s as small as possible, one should work with $L_s = 4$ at $\beta \approx 2.3$. Therefore our initial calculation of glueball masses was on $4^3 \cdot 8$ and 6^4 lattices at $\beta = 2.3$. The time extent was chosen larger so that (69) should be satisfied.

If one then wants to check for continuum behaviour by calculating the glueball masses at β values around $\beta = 2.3$ and seeing if they are indeed independent of β, it is clear from Fig. 7 that we should work at $\beta \geq 2.2$ and that L_s should be greater than 4. If one wants to go as high as, say, $\beta = 2.5$, then L_s should be chosen close to 8. Hence our calculation to check for the renormalization group behaviour of the glueball masses will be performed on an 8^4 lattice.

Another reason for not working at values of β less than 2.3 is the existence of a specific heat peak at $\beta = 2.1 - 2.2$. [42] This is a reflection of a not-too-distant critical point, and there is the danger that the spectrum will be affected in its vicinity. This peak can be seen in Fig. 8 where we plot

$$\sigma = \left(\langle (\tfrac{1}{2} \overline{Tr\ \square})^2 \rangle - \langle \tfrac{1}{2} \overline{Tr\ \square} \rangle^2 \right)^{\frac{1}{2}} \tag{71}$$

versus β for an 8^4 lattice. Here the bar denotes the average over a single lattice configuration, and the brackets denote an average over all the configura-

tions at the given β.

Glueball masses on $4^3 \cdot 8$ and 6^4 lattices

In this section we summarize the results obtained on $4^3 \cdot 8$ and 6^4 lattices. Most of the data was taken at $\beta = 2.3$. We also have some data at $\beta = 2.5$, but most of the results there are not significant.

Some of the data presented here has already been reported on elsewhere [7]. We repeat it here, together with previously unpublished numbers, for the sake of completeness.

The loops used to form our $\vec{p} = 0$ wave-functionals are shown in Fig. 9. (The $F\tilde{F}$ operators are not explicitly drawn due to their complexity; they are defined below). The reader will note that several of the operators ((f) to (i)) have an explicit geometric handedness. This will enable us to construct wave-functionals of both positive and negative parity. The reader will also note that while we employ linear combinations of loops, we do not use products of such loops. This is because such a product has the form of (colour singlet) · (colour singlet), and we would expect it to possess a large continuum cut projection. This expectation will be shown to be correct in some calculations presented later on in this paper.

Using these loops we calculate Γ_a/Γ_0 and Γ_{2a}/Γ_a for the states

$$J^P = 0^+,\ 0^-,\ 1^+,\ 1^-,\ 2^+,\ 2^-,\ 3^+ \ . \tag{72}$$

We obtain statistically significant mass estimates from Γ_{2a}/Γ_a for the 0^+, 0^-, 2^+, 2^- states. For the other states we only get upper bounds on the mass (from Γ_a/Γ_0). We now present our results.

(a) 0^+, 2^+ and 2^-

The 0^+ and 2^+ wave functionals are constructed from all the operators, except $F\tilde{F}$, in Fig. 9. They are constructed as outlined previously. For the 0^+ add all possible orientations and for the 2^+ subtract loops that are orthogonal. To obtain the 2^+ from a loop with a geometric handedness, we add loops of opposite handedness (while preserving the minus sign under rotations of $\pi/2$ about the quantization axis), and to get the 2^- we subtract them. So the 2^- is formed from the basic loops (f-h) in Fig. 9.

In Tab. 2 we present the values of Γ_a/Γ_0 for the 0^+, 2^+, 2^- states for the various loops on the $4^3 \cdot 8$ lattice at $\beta = 2.3$. Our data on the 6^4 lattice uses loops (a) and (h). The values of Γ_a/Γ_0 are similar to those in Tab. 2 except for the 0^+ (h) operator, where the value is $\Gamma_a/\Gamma_0 = 0.19 \pm 0.003$. This is presumably a finite size effect, since the operator (h) is large for an $L_s = 4$ lattice. We find a similar effect when we compare the 0^+(c) loop on the $4^3 \cdot 8$ and 8^4 lattices. What is perhaps surprising is that the finite size effects are so small.

The maximum value of Γ_a/Γ_0 gives an upper bound on the corresponding mass. We find comparing all our results (including arbitrary linear combinations of (a-c) and (f,g) separately):

$$\begin{aligned} m(0^+) &\lesssim (4.88 \pm 0.15)\,\Lambda_{mom} = 1.44 \pm 0.04 \text{ GeV}, \\ m(2^+) &\lesssim (8.53 \pm 0.27)\,\Lambda_{mom} = 2.51 \pm 0.08 \text{ GeV}, \\ m(2^-) &\lesssim (11.38 \pm 0.20)\,\Lambda_{mom} = 3.35 \pm 0.06 \text{ GeV}. \end{aligned} \tag{73}$$

To obtain the actual mass estimate we use Γ_{2a}/Γ_a. To reduce the contamination of Γ_{2a}/Γ_a by higher mass states it is best to confine ourselves to the operators with largest Γ_a/Γ_0; (b,c,h) for the 0^+, (a,b,c,h) for the 2^+, and (f,g,h) for the 2^-. We obtain:

$$m(0^+) = (3.6 \pm 0.35)\Lambda_{mom} = 1.07 \pm 0.11 \text{ GeV},$$

$$m(2^+) = (6.5 \,{}^{+\,1.8}_{-\,1.1})\Lambda_{mom} = 1.92 \,{}^{+0.53}_{-0.32} \text{ GeV}, \qquad (74)$$

$$m(2^-) = (5.5 \,{}^{+\,2.5}_{-\,1.3})\Lambda_{mom} = 1.63 \,{}^{+0.75}_{-0.38} \text{ GeV}.$$

In converting Λ_{mom} to GeV units we have used our measured value of the string tension

$$\sqrt{K} = 1.47\,\Lambda_{mom} \qquad (75)$$

at $\beta = 2.3$ (which is consistent with previous results [6]) and have put in $\sqrt{K} = 430$ MeV. In evaluating (74) we note that the small value of Γ_a/Γ_0 for the 2^- suggests its real mass will be at the top end of the quoted error range.

In Fig. 10 we plot Γ_{2a}/Γ_a as a function of the number of iterations for the 0^+ $\vec{p} = 0$ wave-functional formed from the 1 x 2 plaquette. This illustrates the appearance of statistical errors in our calculations.

(b) 1^+, 1^- and 3^+

For these states we have no significant results for Γ_{2a}/Γ_a. Our results on Γ_a/Γ_0 are presented in Tab. 3. They provide the upper bounds:

$$m(1^+) \lesssim (14.6 \pm 0.4)\Lambda_{mom} = 4.3 \pm 0.1 \text{ GeV},$$
$$m(1^-) \lesssim (12.8 \pm 0.4)\Lambda_{mom} = 3.8 \pm 0.1 \text{ GeV}, \qquad (76)$$
$$m(3^+) \lesssim (13.0 \pm 0.6)\Lambda_{mom} = 3.8 \pm 0.2 \text{ GeV}.$$

Given the coarseness of our lattice one need not regard these numbers as being very relevant to continuum physics.

(c) 0^-

For this state we use two classes of wavefunction. The first class, (f-h) in Fig. 9, consists of purely space-like loops with a geometric handedness. The second class of wavefunctions possess an extension in time and are variations on the $\tilde{F}F \equiv \epsilon_{\mu\nu\rho\sigma} F_{\mu\nu} F_{\rho\sigma}$ continuum operator ("$\vec{E}\cdot\vec{B}$"). We employ two versions [43]:

$$(F\tilde{F})_1 = \sum_{\mu,\nu,\rho,\sigma=\pm1}^{\pm4} \tilde{\epsilon}_{\mu\nu\rho\sigma}\, \mathrm{Tr}\,[U_\mu(n)\, U_\nu(n+e_\mu)\, U_\rho(n+e_\mu+e_\nu)$$
$$U_\sigma(n+e_\mu+e_\nu+e_\rho)\, U^+_\mu(n+e_\nu+e_\rho+e_\sigma)\, U^+_\nu(n+e_\rho+e_\sigma)\, U^+_\rho(n+e_\sigma)\, U^+_\sigma(n)] \qquad (77)$$

and

$$(F\tilde{F})_2 = \sum_{\mu,\nu,\rho,\sigma=\pm1}^{\pm4} \tilde{\epsilon}_{\mu\nu\rho\sigma}\, \mathrm{Tr}\,[U_{\mu\nu}(n)\, U_{\rho\sigma}(n)], \qquad (78)$$

where $U_\mu(n)$ is the matrix along the link in the μ direction leaving the site n, and $U_{\mu\nu}(n)$ is the matrix associated with a plaquette open at the site n, and obtained by going first in the μ and then in the ν direction. The values of μ, etc. are extended to include -1 to -4, where the negative value, $-|\mu|$, denotes going out of the site n in the negative μ direction. The $\tilde{\epsilon}_{\mu\nu\rho\sigma}$ tensor coincides with $\epsilon_{\mu\nu\rho\sigma}$ for all indices positive and is extended to negative values by the definition $\tilde{\epsilon}_{-1\nu\rho\sigma} = -\tilde{\epsilon}_{1\nu\rho\sigma}$, etc. In these definitions we follow ref. (43).

These $\tilde{F}F$ objects are clearly 0^-. They remain 0^- without the time antisymmetrization, and sometimes we use them so. One reason for turning to these rather cumbersome loops is that we find, in fact, no significant signal for Γ_{2a}/Γ_a using the purely space-like loops in Fig. 9 (f-h). In addition $\tilde{F}F$ is a 0^- operator that appears in the (general form of the) QCD Lagrangian and so is a natural choice for the 0^- glueball just as $F_{\mu\nu}F_{\mu\nu}$ is a natural choice for the 0^+ glueball.

In using these $\tilde{FF}$ operators it is important to recall that the positivity [26] of the Wilson action tells us that the following correlation function is positive when the two operators do not overlap:

$$\langle O(t)\ R_t\ O(o)\rangle \geq 0, \tag{79}$$

where R_t reflects the operator in time. Since our $\tilde{FF}$ operators are odd under time reflection, but since the square of the operator is always positive, we have

$$\begin{aligned}
&\langle \tilde{FF}(o)\ \tilde{FF}(o)\rangle \geq 0\ , \\
&\langle \tilde{FF}(a)\ \tilde{FF}(o)\rangle \quad ?\ , \\
&\langle \tilde{FF}(2a)\ \tilde{FF}(o)\rangle \leq 0?\ , \\
&\langle \tilde{FF}(t \geq 3a)\ \tilde{FF}(o)\rangle \leq 0\ .
\end{aligned} \tag{80}$$

The question mark denotes the fact that Γ_a and Γ_{2a} involve time-overlapping operators, so it is not clear what sign to expect. In fact the overlap of the operators in Γ_{2a} is so small that it can probably be ignored and we expect $\Gamma_{2a} \leq 0$. Our measurements confirm this pattern.

Since we want to use Γ_{2a}/Γ_a for the mass estimate, we would like to reduce the operator overlap. To do so we note that if we just use the positive time piece of $(\tilde{FF}(t))_1$, it looks like a 0^- operator centered at time $t + a/2$. Such an operator reflects into itself and will produce no overlap in Γ_{2a} and minimal overlap in Γ_a.

The calculation of these operators is very slow, and the time required to obtain a reasonable signal/error ratio using $\vec{p} = 0$ wavefunctions would have been prohibitive. The solution to this problem, as discussed previously, is to use momentum smeared wavefunctions: specifically our wavefunction consists of a nearest neighbour sum of truncated $(\tilde{FF})_1$ terms (as above). The calculation

is on a 6^4 lattice at $\beta = 2.3$.

From Γ_{2a}/Γ_a we obtain an energy

$$E^2 \approx m^2 + \overline{p^2}\ , \tag{81}$$

where $\overline{p^2}$ represents the unknown momentum smearing. To determine $\overline{p^2}$ we do the same calculation for the 0^+ and 2^+ and use the previously established values. We find

$$m(0^-) = (6.5 \pm 1.1)\Lambda_{mom} = 1.77 \pm 0.3\ \text{GeV} \tag{82}$$

with an upper bound from Γ_a/Γ_0 of

$$m(0^-) \leq (8.04 \pm 0.23)\Lambda_{mom}\ . \tag{83}$$

From the space-like operators (f-h) we obtain a much less useful upper bound

$$m(0^-) \leq (11.9 \pm 0.8)\Lambda_{mom}\ . \tag{84}$$

The space-like 0^- operators appear not to have any significant projection onto the lowest 0^- state seen using the $\tilde{FF}$ operators as wave-functionals.

(d) $\beta = 2.5$

At $\beta = 2.5$ we find that our wave-functionals have become very poor, and we have no useful numbers for the masses beyond the upper bounds

$$\begin{aligned}
m(0^+) &\leq (6.8 \pm 0.4)\Lambda_{mom}\ , \\
m(2^+) &\leq (9.1\ {}^{+\ 2.1}_{-\ 1.5})\Lambda_{mom}\ .
\end{aligned} \tag{85}$$

Masses and renormalization group behaviour on an 8^4 lattice

In performing our calculation on the $4^3 \cdot 8$ (and 6^4) lattice we were careful to satisfy, as well as we could, the obvious physical requirements (68,69) for being in the continuum limit. However, in order to work on as spatially small a lattice as possible, we actually satisfy these requirements with weak rather than strong inequalities. The fact that scaling behaviour of the string tension has already set in at this value of β [6] suggests that this is enough. Nonetheless additional evidence is required to support the assertion that our results pertain to the continuum limit. To do so we have recalculated [9] the 0^+ and 2^+ masses on an 8^4 lattice for $\beta = 2.2$, 2.3 and 2.4. For these values of β an 8^4 lattice is a large lattice, see Fig. 7.

To be able to perform these calculations in a reasonable time we used momentum smeared wavefunctions. To be specific, we summed our basic wavefunction over a 3^3 block of adjacent equal-time sites to give a single wave-functional. At each time we split the 8^3 sites into 27 such blocks (so there is minimal overlap), so that each time slice now gives us 27 measurements rather than just one. The price we pay is that Γ_{2a}/Γ_a now gives us an energy, E, rather than a mass, since the wavefunction is not completely translation invariant and hence contains $\vec{p} \neq 0$ components. However, since the wave-functionals have a rather large spatial extension, this momentum smearing should be reasonably small. If it is small compared to the mass, then we can use the relation

$$E^2 = m^2 + \delta^2/a^2 \qquad (86)$$

to parameterise the energy obtained from Γ_{2a}/Γ_a in terms of the mass and an average momentum $\overline{p^2} = \delta^2/a^2$. The momentum $\overline{p^2}$ has an a^{-2} dependence, because the size of our wavefunction is fixed in units of a.

The use of (86) will be accurate as long as the mass term dominates. This needs to be checked, and we will do so below. We shall see that the heavier 2^+ meson is wholly insensitive to the presence of $\overline{p^2}$. So we shall have to estimate $\overline{p^2}$ using the 0^+ measurements.

The results we summarize come in three parts. In the first part we calculate $m(0^+)$ and $m(2^+)$ using only the 8^4 data, but assuming the masses are independent of β. In the second part we put together the 8^4 and $4^3 \cdot 8$ data and check that indeed the masses do not vary with β. In the third part we check for finite size effects.

For a calculation of the wavefunction projection onto the lowest 0^+, 2^+ glueballs we refer to ref. (10), where the expected rapid worsening of this projection with increasing β is demonstrated.

(a) $m(0^+)$ and $m(2^+)$

The basic loops we use are the 1 x 1 and 2 x 2 plaquettes in the by now familiar linear combinations. We take our 0^+ results for Γ_{2a}/Γ_a at $\beta = 2.2$, 2.3, 2.4 and use them to obtain the corresponding energies. We transform all lattice spacings to $a(\beta = 2.3) \equiv a$, express the energies as in equ. (86) and solve for $m(0^+)$ and δ :

$$m(0^+) \cdot a = 1.15 \begin{matrix} +0.11 \\ -0.22 \end{matrix} , \qquad (87)$$

$$\delta^2 = 1.5 \begin{matrix} +0.5 \\ -0.3 \end{matrix} . \qquad (88)$$

We now use this δ^2 and our 2^+ values of Γ_{2a}/Γ_a to obtain

$$m(2^+) \cdot a = 2.46 \begin{matrix} +0.07 \\ -0.21 \end{matrix} . \qquad (89)$$

These results are consistent with our previous results on smaller lattices and reveal the absence of large finite size effects.

(b) renormalization group behaviour

We want to demonstrate now that our 0^+ and 2^+ masses are in fact independent of β in the range 2.2 to 2.4. We take our previous estimate, on a $4^3 \cdot 8$ lattice, of the 0^+ mass at $\beta = 2.3$ and combine it with our energy measurement on the 8^4 lattice at $\beta = 2.3$ to extract δ^2 (using equ. (86)):

$$\delta^2 = 1.35 \begin{matrix} + .29 \\ - .32 \end{matrix} . \qquad (90)$$

We use this value of δ^2 in conjunction with (86) and our other measurements on the 8^4 lattice to obtain the masses of the 0^+ and 2^+ glueballs at $\beta = 2.2$ and $\beta = 2.4$ as shown in Fig. 11. We observe that the masses are indeed independent of β within the statistical errors. The lattice spacing changes by a factor of about 1.7 between $\beta = 2.2$ and 2.4, while the errors could hide a change of perhaps at most $\simeq 20$ %. Hence the scaling result we have is significant.

(c) finite size effects

Our mass measurements show no finite size effects within the errors. To search for small changes and/or wavefunction effects we compare our measurements of Γ_a / Γ_0 for $\vec{p} = 0$ 0^+ and 2^+ operators based on 1 x 1 and 2 x 2 plaquettes on lattices of sizes 4^4, $4^3 \cdot 8$, 6^4 and 8^4. This is shown in Fig. 12. We observe no significant finite size effects except for the 2 x 2 0^+ operator, and even there the change is only $\simeq 20$ %.

Finally we return to the question of how good is equ. (86). As we remarked this will be accurate to the extent that E/m is close to unity. We now have the information to perform the necessary consistency check on our results. Taking our calculated masses in equs. (87) and (89) and taking our measured energies, we plot in Fig. 13 the ratio E/m for 0^+ and 2^+ as a function of β. We see that the 2^+ meson is insignificantly effected by the momentum smearing, and that even for the 0^+ equ. (86) should be reliable.

Glueball masses in the Hamiltonian limit

In this section we describe results obtained on a lattice with a very small temporal lattice spacing:

$$a_t \ll a_s , \qquad (91)$$

which we may regard as a good approximation to the Hamiltonian formulation of lattice gauge theory. The Hamiltonian formulation is conceptually closer to the continuum theory, and the propagation in time of our glueballs– mutilated though they may be through the spatial discretization– is as in the continuum theory.

The primary motivation is to obtain a finer grained picture of the glueball correlation functions, both to check explicitly that beyond some distance the correlation functions are indeed dominated by a single glueball of non-zero mass and to obtain some information on higher-mass excited states. One can also use such an asymmetric lattice to obtain a rough estimate of heavy glueball masses very quickly, as if one were to measure, say, $\Gamma_a / \Gamma_{a/2}$ on one of our previous lattices. This would be important in a dedicated variational calculation as discussed in the introduction.

One of further advantages concerns glueballs such as the 0^-, whose wave-functions have a temporal extent. This temporal extent should obviously be much less than the time extent over which the correlation function is measured: the time extent in the wave-functional represents a time derivative in the continuum (and hence an infinitesimal time interval), whereas the time in the correlation function really does represent some fixed time interval. On the usual hypercubic lattice it is not really possible to satisfy such a condition. Here we can.

A further motivation for such a calculation is that it provides a check on the sensitivity of our results to changes in the action, i.e. to changes in our manner of approaching the continuum limit.

(a) formulation

The scales of a lattice are determined by the values of the coupling. So in order to have different temporal and spatial scales one must introduce two couplings into the action

$$\beta \sum_{\text{all}} \mathrm{Tr}\,\square \;\longrightarrow\; \beta_s \sum_{\text{spatial}} \mathrm{Tr}\,\square + \beta_t \sum_{\text{temporal}} \mathrm{Tr}\,\square \,. \qquad (92)$$

Suppose we want to achieve a ratio

$$a_t/a_s = r \,, \qquad (93)$$

and suppose β is the coupling appropriate to the hypercubic lattice with $a = a_s$. Then ignoring perturbative corrections for the action to give the correct continuum limit we require

$$\beta_s = r\beta \,, \quad \beta_t = \beta/r. \qquad (94)$$

The perturbative corrections are small and have been calculated in ref. (44). We wish to have $\beta = 2.3$ and $r = 0.25$. According to the calculations of ref. (44) this means taking

$$\beta_s = 0.664 \,, \quad \beta_t = 8.5 \,. \qquad (95)$$

We shall work with (95) on a $5^3 \cdot 40$ lattice. Thus the temporal extent corresponds to about 90 MeV which is well in the confining phase. The spatial extent is 5 rather than 4 lattice spacings so as to provide a safety margin.

Before proceeding to the main calculation we check to make sure that the perturbatively motivated couplings (95) are indeed in the right ball-park. To do so we measure the correlation function of parallel plaquettes, ϕ, in both the spatial and time directions, i.e. $\langle \phi(\vec{x},\, t+na_t)\,\phi(\vec{x},t)\rangle$ and $\langle \phi(\vec{x}+na_s,t)\,\phi(\vec{x},t)\rangle$, where the orientation of the ϕ is such that they face each other, and the vacuum expectation value has been removed. We measure these correlation functions on our old $4^3 \cdot 8$ lattice at $\beta = 2.3$ as well as on our current $5^3 \cdot 40$ lattice at $\beta_s = 0.664$, $\beta_t = 8.5$. A comparison of the large distance behaviour of these correlation functions should allow us to compare the scales. In Tab. 4 we present the results based on about 1000 lattice configurations in each case. The results are consistent with

$$a_s \approx a(\beta = 2.3) \,, \quad a_s \approx a_t \cdot (3.5 - 4.0). \qquad (96)$$

We now proceed with our main calculation.

(b) glueball correlation functions

0^+

We use a $\vec{p} = 0$, 0^+ wave-functional constructed out of 2x2 plaquettes. In the usual fashion we add all such 2x2 squares at a given time. The correlation functions are measured on 15000 gauge field configurations of our $5^3 \cdot 40$ lattice. These configurations were produced in two sequences, one from an ordered ($\beta = \infty$) and one from a disordered ($\beta = 0$) starting configuration. No differences were observed between these sequences within the statistical errors. The same is true of our other data on this lattice.

In Fig. 14 we plot the 0^+ correlation function Γ_{na_t}/Γ_0 out to 12 lattice spacings, and in Tab. 5 we give the actual numbers. For $n \gtrsim 4$ the data falls on a single exponential. This can be seen better by calculating the local exponent. This we do by the formula

$$m(n) = 3.5 \ln \left[\frac{\Gamma_{(n-1)a_t}}{\Gamma_{na_t}} \right] . \qquad (97)$$

The factor of 3.5 may at this moment be viewed as an arbitrary overall normalization factor. It represents, as we shall later argue, an estimate of the factor required to take us from our old lattice spacing at $\beta = 2.3$ to a_t. Hence m(n) can be compared to our previous results on $m \cdot a$. Ignoring this for now, we plot m(n) in Fig. 15 and observe the very clear dominance of the long distance ($n \gtrsim 4$) correlation function by a state of non-trivial mass.

Does this prove that the theory really has a non-zero mass gap? Another much more obscure suggestion is that there may be no clear pole but just a cut. Our data demonstrates that such a cut would have its branch point at $m \approx 1$ (in the

units of our figure), and that this branch point would have to be singular so as to dominate the correlation function from small distances. That is to say the cut would have to look like a pole at its branch point. All this seems very unlikely, and our data points very clearly to the existence of a non-trivial mass gap and pole in the 0^+ channel.

0^+ recurrences

The fine-grained data we now possess invites an attempt to determine the next higher excited state in this channel. It is obvious that only a crude determination is possible. Any states which are close in mass will be effectively degenerate for our purposes. The best we can search for is the dominant range of masses beyond that around the lowest mass. The kind of fit we therefore attempt is as follows. On the basis of Fig. 15 we assume the contribution of the higher mass state to Γ_{na_t} for $n \gtrsim 4$ to be negligible. The fit with two masses should be a good fit to Γ_{na_t} for $n \gtrsim 2$, and all of the Γ's should be well fitted by the inclusion of a third mass (although a third mass may not be necessary). The functional form of the fit is

$$\frac{\Gamma_{na_t}}{\Gamma_0} \equiv \alpha e^{-mna_t} + \beta e^{-m'na_t} + \gamma e^{-m''na_t} \qquad (98)$$

(subject to the above stated constraints). Typical values of the parameters turn out to be

$$\begin{aligned} \alpha &= 0.35 - 0.40 \ , \quad ma_t = 0.33, \\ \beta &= 0.40 - 0.60 \ , \quad m'a_t = 1.11 - 1.51, \\ \gamma &= 0. \ - 0.20 \ , \quad m''a_t \gtrsim 2.4, \end{aligned} \qquad (99)$$

so we estimate the excited 0^+ mass, m', to be

$$m'/m = 4.0 \pm 0.6 \qquad (100)$$

in terms of the lowest glueball mass m. The error in (100) is only a crude estimate. One might worry that on a small lattice such a high mass might be purely a lattice artifact. We point out, however, that the time-like cut-off energy is π/a_t, which is about 2.5 times larger than m', and so while m'' is surely not to be taken seriously, we believe that m' is indeed relevant to continuum physics, although one should bear in mind that it might well correspond to, say, $J^P = 4^+$ rather than 0^+.

2^+

As for the 0^+ we use a $\vec{p} = 0$ wave-functional constructed out of 2x2 plaquettes, except now we do not sum all the plaquettes but instead take the difference of orthogonal planes to construct a 2^+ operator in the usual way.

The discussion is just as for the 0^+ case. In Fig. 16 we plot the 2^+ correlation function Γ_{na_t}/Γ_0 out to 12 lattice spacings, and in Tab. 5 we give the actual numbers. In Fig. 17 we plot the effective mass versus distance using (97). Beyond n = 8 the errors become very large on this linear scale, so we do not show the data beyond n = 8. We conclude, as for the 0^+ (though with somewhat weaker statistical significance), that we see a non-trivial mass gap in the 2^+ channel.

2^+ recurrences

Again we can attempt to obtain an estimate of the next excited mass. Using a fit as in (98) with the same criteria we find typical values of the parameters to be

$$\begin{aligned} \alpha &= 0.35 \quad , \quad ma_t = 0.63, \\ \beta &= 0.60 - 0.70 \quad , \quad m'a_t = 1.61 - 1.72, \\ \delta &= 0. \ - 0.10 \quad , \quad m''a_t \gtrsim 2.6. \end{aligned} \tag{101}$$

So we estimate the excited 2^+ mass, m', to be

$$m'/m = 2.6 \pm 0.1 \ . \tag{102}$$

This mass, although high, is again about a factor of 2 lighter than the cut-off energy and hence should be significant.

0^-

For the 0^- we use a $\vec{p} = 0$ wave-functional based on the $\tilde{F}\tilde{F}$ operator defined in (78). This operator is rather slow to calculate with, and so we calculated wave-functionals only for even times. Hence we have available only Γ_0, Γ_{2a_t}, Γ_{4a_t}, etc. Since the 0^- mass is close to that of the 2^+, we anticipated obtaining results comparable to those of the 2^+ in statistical accuracy. Thus we expected to have statistically useful results on such ratios as $\Gamma_{6a_t}/\Gamma_{4a_t}$ and $\Gamma_{8a_t}/\Gamma_{4a_t}$ for which all time intervals are large compared to the time extension of the $\tilde{F}\tilde{F}$ operator, so that systematic errors due to this extension would be minimal.

The surprise was that the statistical fluctuations turned out to be much larger than in our previous calculations based on hypercubic lattices. This can be understood as follows. It is clear that the internal cancellations in $\tilde{F}\tilde{F}$ between the positive time and negative time pieces becomes more important as the lattice spacing decreases. To attempt to salvage this situation we also began to calculate with two other variations on the full $\tilde{F}\tilde{F}$ operator (called FFD from now on). The first variation was to take just the positive time piece of $\tilde{F}\tilde{F}$ at time t and calculate the correlation function with the negative time piece at time $t' < t$ as in Fig. 18a. This has the advantage of decreasing the time extension and the overlap of operators and hopefully the statistical fluctuations. We refer to it as FFU. The second variation is to do the same only with $t' > t$ and then to add FFU to it as in Fig. 18b. We call this FFDU.

For FFD we have measurements on 9000 lattice configurations, for FFU on 3000 configurations and for FFDU on 6000 configurations.

Our data is tabulated in Tab. 6, and in Fig. 19 we plot the FFD correlation function. The largest n for which we have small statistical errors is n = 4. So we make our mass estimate from $\Gamma_{4a_t}/\Gamma_{2a_t}$. For such small n the admixture of higher masses, especially in Γ_{2a_t}, is probably significant. This is certainly the case for the 2^+ glueball. In the spirit of the variational calculation we obtain a mass estimate from $\Gamma_{4a_t}/\Gamma_{2a_t}$ for each of our three operators and take the lowest mass to be the best estimate. This turns out to be for the FFU operator, and the mass estimate is

$$ma_t = 0.59 \pm 0.06 \ . \tag{103}$$

In terms of the 0^+ glueball mass we find

$$\frac{m(0^-)}{m(0^+)} = 1.8 \pm 0.2 \ , \tag{104}$$

which is consistent with our earlier results. A more detailed comparison will be given later.

We note that the construction of the FFU wave-functional is such that there are no overlapping operators in $\Gamma_{4a_t}/\Gamma_{2a_t}$, and the intervals over which the correlations are taken are large compared to the time extension of the wave-functional itself. Thus this 0^- mass estimate removes the theoretical uncertainties afflicting our previous measurements of the 0^- mass. In addition the estimate has the advantage of using $\vec{p} = 0$ rather than momentum-smeared wave-functionals.

The mass estimate in (103) is consistent with our data at larger n (within errors). Moreover, our three estimates of the mass using $\Gamma_{4a_t}/\Gamma_{2a_t}$ (0.59 ± 0.06, 0.71 ± 0.06, 0.69 ± 0.05 for FFU, FFD, FFDU respectively) are so close together that the error due to higher mass admixtures is likely to be well within the quoted statistical errors.

(c) glueball masses and previous results

mass ratios

In Fig. 20 we plot our results for the ratio of the 2^+ to 0^+ masses taken on three different lattices. The results are in very satisfactory agreement. In Fig. 21 we plot the ratio of 0^- to 0^+ masses. Again all the data are consistent. For comparison we plot the SU(3) results (to be discussed in the companion paper [8,11](II)). The results are very similar to those of the SU(2) theory. If $N_c = 3$ is close to $N_c = \infty$, then so is $N_c = 2$!

At least as far as the mass ratios are concerned the data in Figs. 20, 21 provide evidence that systematic errors afflicting our calculations are small.

normalization

The perturbative expressions for the couplings tell us that

$$a_t = 0.25a, \tag{105}$$

where a is the hypercubic lattice spacing at $\beta = 2.3$. We cannot, however, expect (105) to be exact because of higher order corrections. Our earlier calculation with parallel plaquettes confirmed that (105) is not a bad approximation. In fact we found that, roughly,

$$a_t \simeq (0.25 - 0.29)\ a \ . \tag{106}$$

Can we do better now?

Let $a = ra_t$. Then we can compare $\Gamma_{ra_t}/\Gamma_{ra_t/2}$ to our old Γ_{2a}/Γ_a, and $\Gamma_{ra_t/2}/\Gamma_o$ to our old Γ_a/Γ_o. The latter measurement provides a weaker criterion since it involves the wavefunctions and higher mass states as well. We show the results of such a comparison in Tab. 7. The data for 0^+ and 2^+ glueballs has been transformed into the $\beta = 2.3$ ratios Γ_a/Γ_o and Γ_{2a}/Γ_a for r = 3.5 and r = 4 (using $\Gamma_{3.5a_t} = (\Gamma_{3a_t}\cdot\Gamma_{4a_t})^{1/2}$) and compared to our previous data on the $4^3\cdot 8$ and 8^4 lattices. Note that the data on Γ_{2a}/Γ_a for the 8^4 lattice involves data at $\beta = 2.2$, 2.3 and 2.4 transformed to $\beta = 2.3$ by the usual perturbative formula for β. The Γ_a/Γ_o data is all from $\beta = 2.3$.

We see that relying on Γ_{2a}/Γ_a alone tells us that $r \in [3.5, 4]$. If we include Γ_a/Γ_o into our considerations, then r = 3.5 is preferred.

Using $r \in [3.5, 4]$ it is now of interest to ask how good was our technique of estimating the mass using Γ_{2a}/Γ_a. The error arises because, as we can see from our effective mass plots in Figs. 15, 17, Γ_a $\left(\approx (\Gamma_{3a_t}\cdot\Gamma_{4a_t})^{1/2}$ or $\Gamma_{4a_t}\right)$ still possesses some contamination from higher mass states. A detailed examination shows that the "true" mass is O(5 %) less for the 0^+ and O(8 %) less for the 2^+ than that which we would obtain from Γ_{2a}/Γ_a. This number lies within our typical statistical errors, and hence we have confirmed that using Γ_{2a}/Γ_a to obtain masses on a hypercubic lattice at $\beta = 2.3$ is indeed an accurate prescription.

(d) continuum correlation functions

Our 2^+ glueball mass is approximately twice the 0^+ glueball mass. One may ask

whether it is possible that we are seeing not a 2^+ glueball but simply the 2^+ partial wave of the two-0^+ glueball continuum. In the case of the 2^+ it is in fact obvious that such a possibility is most implausible. Since the piece of the wavefunction that is at our 2^+ glueball mass is $\simeq$40 %, a reinterpretation in terms of a continuum cut would require the same $\simeq$ 40 % projection to be onto the tip of the cut, whereas we would actually expect very little such projection because of angular momentum suppression factors. Nonetheless it would be interesting to see how a continuum cut contributes to a correlation function, since some of the higher spin states are considerably heavier than the sum of two 0^+ glueball masses.

In this section we shall construct wave-functionals that have a large projection onto the two-glueball continuum. To do so, we deliberately use operators that are products of loops.

We shall construct two 0^+ continuum correlation functions and two 2^+ continuum correlation functions. All use the 2x2 plaquette as their basic component. The first 0^+ wave-functional, labelled RPR00, is constructed as follows. Form a 0^+ wave-functional centred on the point $\vec{x}$ by summing all the 2x2 spacelike plaquettes centred on $\vec{x}$ and subtracting the vacuum expectation value. Now square it and sum over all points $\vec{x}$ at a given time. Our second 0^+ wave-functional is constructed in the same way except that instead of squaring a 0^+ operator at $\vec{x}$, we square a 2^+ operator. We call this RPR22 (the vacuum expectation value is subtracted). Our first 2^+ "continuum" operator, call it WPR02, is constructed as above except that at each point $\vec{x}$ we multiply a 0^+ with a 2^+ wave-functional. Our second 2^+ operator, call it WPRL2, is a little more complex. Choose a point $\vec{x}$. Multiply the 0^+ operator about $\vec{x}$ by the 0^+ operator about $\vec{x}' = \vec{x} + \vec{e}_i a + \vec{e}_j a$. Now multiply the 0^+ operator about $\vec{x}'' = \vec{x} + \vec{e}_i a$ by the one about $\vec{x}''' = \vec{x} + \vec{e}_j a$.

Subtract the two products from each other and sum over all $\vec{x}$ at fixed time.

We have measured the correlation functions associated with these wave-functionals, and the results are shown in Fig. 22a-d. The curves represent "fits" which we shall explain presently. First we outline what we might expect to find with these measurements. The continuum projection will be across some range of masses, and as n increases Γ_{na_t} will be increasingly dominated by masses nearer the cut. The effective mass, m(n), as defined earlier should therefore start at high values and decrease gradually. For the 0^+ "continuum" wave-functional, if there is any projection onto the 0^+ glueball pole, this should dominate at larger n. In the 2^+ wave-functional there will be no 0^+ pole, but there can be a 2^+ glueball pole. This will be much less clear, since this pole will be competing with the tip of the cut. Its only advantage is that it will be free of any angular momentum suppression factors. So it should show up eventually. A further feature we would look for in comparing the two types of continua is the presence of these angular momentum suppression factors. All other things (i.e. dynamics) being equal we expect an extra factor of $q^{2L} = q^4$ (for L = 2) in the 2^+ case, where q is the centre of mass momentum. If m_c is the threshold of the cut, then

$$q^2 = m^2 - m_c^2 \underset{m \approx m_c}{\approx} (m - m_c)\, 2m_c \ . \qquad (107)$$

We now turn to our data. We have in general

$$\frac{\Gamma_{na_t}}{\Gamma_0} = \int dm\ \alpha(m)\ e^{-m n a_t} \ , \qquad (108)$$

and we parameterise $\alpha(m)$ by a pole and cut term

$$\alpha(m) = \alpha_0\, \delta(m-m_p) + \alpha_1\, \theta(m-2m_0)\,(m-2m_0)^{\beta}\, e^{-\lambda m} \ . \qquad (109)$$

Here m_p is the pole position, m_o is the 0^+ glueball mass (so $2m_o$ is the threshold of the cut) and the cut discontinuity is parameterised by a function that can vanish at threshold (depending on β) and dies away exponentially at large masses (α_1 is determined by the condition $\Gamma_{na_t=0} / \Gamma_o = 1$). Actually there are many cuts, e.g. the three 0^+ glueball cut, and our parameterisation does not try to be realistic in detail. Neither do we attempt precise fits. We are searching for rather gross features of the data.

If we begin with the 0^+ correlation functions, RPR00 and RPR22, we immediately see at large distances the presence of the 0^+ pole. Indeed for $n \gtrsim 4$ the correlation functions fall exponentially, with the exponent determined by the 0^+ glueball mass. However, they differ from our previous 0^+ correlation functions in that they fall <u>much</u> more steeply at smaller n. The curve through the RPR00 data is using a mass spectrum

$$\alpha(m) = 0.015\, \delta(m-m_o) + \alpha_1\, \theta(m-2m_o)\,(m-2m_o)^2\, e^{-m a_t} \ . \qquad (110)$$

For the solid curve through the RPR22 data we used

$$\alpha(m) = 0.015\, \delta(m-m_o) + \alpha_1\, \theta(m-2m_o)\,(m-2m_o)\, e^{-0.53 m a_t} \ . \qquad (111)$$

The 0^+ pole term has a small coefficient; however, it is necessary. The dashed curve shows what happens when we try to do without it, using

$$\alpha(m) = \alpha_1\, \theta(m-m_o)\,(m-2m_o)^{0.5}\, e^{-0.37 m a_t} \qquad (112)$$

(the reason for an a_t in the exponent is that λ has the dimensions of an inverse mass). The two fits have apparently different mass spectra. However, their

grossest feature is the same: the continuum mass spectrum has a maximum at about $8m_o$ in both cases. This is because the maximum, $\hat{m}$, is given by

$$\hat{m} = 2m_o + \frac{\delta}{\lambda} . \qquad (113)$$

They differ in their threshold behaviour, but the 0^+ pole term takes over before the threshold of the cut dominates. Our intuitive expectation that a product wave-functional would have little projection onto the single colour singlet state has turned out justified.

Consider now the 2^+ correlation functions WPRO2 and WPRL2. We can no longer see any very obvious pole term at large n. However, having a pole term improves the typical fit to the data, typically to the extent shown in Fig. 22d, where the solid curve has a 2^+ pole term ($m = m_2$), while the dashed curve has no such pole. Within the statistical errors the improvement is marginal but probably there. This solid curve in Fig. 22d is based on the mass spectrum

$$\alpha(m) = 0.013\,\delta(m-m_2) + \alpha_1\,\theta(m-2m_o)\,(m-2m_o)^4\,e^{-1.9\,ma_t} , \qquad (114)$$

while the dashed curve comes from using

$$\alpha(m) = \alpha_1\,\theta(m-2m_o)\,(m-2m_o)^3\,e^{-1.56\,ma_t} . \qquad (115)$$

The solid curve in Fig. 22c comes from using

$$\alpha(m) = 0.01\,\delta(m-m_2) + \alpha_1\,\theta(m-2m_o)\,(m-2m_o)^2\,e^{-0.91\,ma_t} . \qquad (116)$$

We observe at most a small projection onto the 2^+ pole, comparable in fact to the previous projection onto the 0^+ pole. Using (113) we see that the continuum mass spectrum peaks at $\hat{m}$, where

$$\hat{m} \approx 8\,m_o \qquad (117)$$

for all the fits. This is the same value as for the 0^+ correlation functions, and we can thus take it to be a "typical" parameter for continuum contributions.

A second feature of the continuum mass spectra concerns the threshold factors. Comparing (110-112) with (114-116) we observe that the 2^+ continuum has an extra threshold factor compared to the 0^+ continuum. Averaging over all the fits it comes to a factor

$$\approx (m - 2m_o)^2 . \qquad (118)$$

If we recall (107), we see that this is precisely what we expect from the L = 2 angular momentum factors for a 2^+ partial wave! How real is this effect? We emphasized earlier that there can be some trade-off between δ and λ in (109). The extent of this trade-off is, however, limited. The $e^{-\lambda m}$ factor is more important to what happens between Γ_o and Γ_{a_t}, while the $(m - 2m_o)^\delta$ factor determines to what extent Γ_{2a_t} deviates from the naive extrapolation of the $e^{-\lambda m}$ behaviour. The smaller is $\Gamma_{2a_t}/\Gamma_{a_t}$ as compared to Γ_{a_t}/Γ_o, the larger will be the required value of δ. So we see that (118) is a real effect. If we compare Fig. 22a,b to Fig. 22c,d we observe that although Γ_{a_t}/Γ_o is comparable in all cases, $\Gamma_{2a_t}/\Gamma_{a_t}$ is smaller for the 2^+ correlation functions, and so a larger δ will be required there.

Finally we turn to the question of how much our 2^+ glueball wave-functionals project onto the continuum. If this continuum piece is similar to the ones we have described above, then we can immediately estimate that any such projection is much less than 5 %. The same is true for the 0^+ glueball wave-functionals. One may perform a similar exercise for higher-spin states as and when they are calculated.

"Glueball" correlation functions at high temperature

It would be interesting to compare the correlation function measurements we have used to display the existence of a non-trivial colour singlet mass gap (in various channels) with the results of a similar calculation in an unconfined phase of the theory, where we expect no colour singlet bound states but presumably would be seeing only the multi-gluon continuum.

The simplest way to enter an unconfined phase of the theory is by raising the physical temperature of our lattice through the deconfining phase transition at $T \approx 200$ MeV [29]. We shall work on a $5^3 \cdot 9$ lattice at the same values of β_s, β_t as in the previous sections

$$\beta_s = 0.664 \ , \quad \beta_t = 8.5 \ . \tag{119}$$

The temperature, T, of this lattice is

$$T = \frac{1}{L_t a_t} = \frac{1}{9 a_t} \approx 400 \text{ MeV} \tag{1209}$$

(very crudely), which is well into the high temperature unconfined phase of the theory. We measure Γ_{na_t}, $n = 0, 1, \ldots, 4$, for 0^+, $2^+ \vec{p} = 0$ wave-functionals constructed out of 2 x 2 plaquettes in the usual fashion. We perform our measurements on 2500 lattice configurations. Note how, because of our use of an asymmetric lattice, we can work with lattices that have large L_t even at high temperature, in contrast to the usual studies, which use $L_t = 2$ or 3 which may distort the physics.

In Fig. 23 we plot the 0^+ and 2^+ correlation functions, and in Figs. 24, 25 we plot the corresponding effective masses

$$m(n) = 3.5 \ln \left[\frac{\Gamma_{(n-1)a_t}}{\Gamma_{n a_t}} \right] \ , \tag{121}$$

both for the present data and for our previous data on the $5^3 \cdot 40$ lattice. Since the time extent of the lattice is now necessarily small in physical units, the correlation functions do not get to be at large distances, and only the grossest differences with our previous data will be visible.

The major difference between our old data at $T \approx 90$ MeV and the new data at $T \approx 400$ MeV is the steady collapse of m(n) in the high temperature phase, with no sign of the levelling off, which by n = 4 is already apparent in the $T \approx 90$ MeV data. If the correlation functions do level off, it is clear that the masses must be less than 500 MeV for both the 0^+ and 2^+. However, there are no signs of an eventual non-zero mass, and indeed if any such mass is $\lesssim 400$ MeV = T, then it is not clear if it is to be regarded as a genuine mass gap. In fact the $T \approx 400$ MeV data is consistent with arising from the simplest parameterisation of a continuum cut with threshold at zero mass. In Fig. 23a the solid curve is the result of using in (108) a continuum mass spectrum

$$\alpha(m) \sim \theta(m) \, e^{-0.5 m a_t} \ , \tag{122}$$

and the curve in Fig. 23b comes from a mass spectrum

$$\alpha(m) \sim \theta(m) \, e^{-0.75 m a_t} \ . \tag{123}$$

The high temperature correlation functions provide a contrast against the claim that our previous correlation functions display a non-trivial mass gap. They also provide a different and interesting way to see the unconfined character of the high temperature SU(2) gauge theory.

III. Discussion

In our calculation of the SU(2) glueball spectrum [7] we have obtained mass estimates for the lowest lying 0^+, 2^+, 0^- and 2^- states (and mass upper bounds for the 1^+, 1^- and 3^+ states). We have tested for the reliability of these numbers in various ways: finite size effects, renormalization group behaviour [9], re-calculating in the "Hamiltonian limit", calculating continuum contributions, calculating for comparison in the high temperature deconfining phase, etc. We have found that our results survive all these tests, and we conclude that they most probably are representative of the continuum theory.

If one wishes to average all our results, see Figs. 20, 21, one will obtain

$$\frac{m(2^+)}{m(0^+)} = 1.94 \, {}^{+0.15}_{-0.10} \quad , \tag{124}$$

$$\frac{m(0^-)}{m(0^+)} = 1.73 \pm 0.20 \quad . \tag{125}$$

These numbers are mass ratios and hence independent of any arguments about setting the overall scale in physical units. Of course, the reader may not wish to perform such an average, since he may regard some of the numbers as being better than others.

The more physically interesting glueball masses are of course the SU(3) ones, which will appear in the companion paper (II). Our results will be based on spatially small lattices (4^3), but we will not have the computer time to perform the kind of checks we have performed here. Since we expect systematic errors not to differ greatly between SU(2) and SU(3), the analysis of this paper will also

serve to substantiate the reliability of our SU(3) results.

We now comment on related work by other groups. The only other attempt to calculate the SU(2) spectrum (as opposed to just the 0^+ mass) was by Falcioni et al. [15] using a systemic variational calculation [28] with Manton's action. The only number they quote is for the 0^+ mass, and that agrees with our estimate. Their lattice spacing is $\lesssim 1.5$ a ($\beta = 2.3$), so they are somewhat further from the continuum. They give no estimate of other masses except that within errors they are consistent with the 0^+ mass. Such a statement is not necessarily inconsistent with our results if their errors are large enough. In any case it is reassuring that a completely different action (albeit one without the desirable positivity properties) should reproduce the same 0^+ mass (see also ref. (21)). Another calculation, using the same variational technique, comes from Berg, Billoire and Rebbi [16]. They calculate only the 0^+ mass but do it over a range of β. For $\beta \gtrsim 2.5$ their mass estimate increases to larger values, confirming our expectation that a dedicated variational calculation becomes rapidly very difficult as β increases. Their mass estimate, for their scaling region of $\beta \lesssim 2.25$ on a $4^3 \cdot 16$ lattice, agrees with our value. Mütter and Schilling [21] estimate the 0^+ mass from the correlation of interior plaquettes to changes in boundary conditions. They find scaling behaviour up to $\beta \simeq 2.4$, and their 0^+ mass agrees with ours. So does that of Michael and Teasdale [19], and that of Engels, Karsch, Satz and Montvay [18] looking at the finite temperature specific heat curve, and Falcioni et al. [20] using the Langevin equation.

The original [12] lattice glueball estimates were with strong coupling expansions in the Hamiltonian formalism. More recently there have been calculations [13] on the Euclidean lattice also. A typical prediction of these calculations is that

$m(2^+)/m(0^+) \approx 1$ against our value of ≈ 2. This is a serious problem for strong coupling extrapolations. Irrespective of whether our results characterize the continuum limit, we certainly claim that they characterize the region $\beta \simeq 2.3$, and this region lies between the strong coupling and deep continuum limits: a strong coupling extrapolation must reproduce our results on the way to the continuum.

Phenomenological bag model estimates [22] display discrepancies with our results.

The calculations described in this paper represent a first step in understanding the low-energy dynamics of non-abelian gauge theories and QCD. The apparent early onset of scaling enables us to do calculations in regions of β, where the glueball is not much larger than the lattice spacing, so that it is not difficult to find reasonably good wave-functionals. To bring a qualitative improvement, the next step must be either a calculation sufficiently deep in the continuum limit so as to give us a truly fine grained picture of the theory's dynamics, or it has to be a calculation with fermion loops. Either direction requires a qualitative increase in the sophistication of one's techniques.

Acknowledgements

Our work has greatly benefitted from the stimulating interest in lattice theories at DESY and Hamburg. We thank H. Joos, M. Lüscher, H.S. Sharatchandra, K. Symanzik, T. Walsh and P. Weisz for useful discussions and comments. The bulk of the calculations were performed at the DESY computer centre. Some of the early calculations were performed on the Wisconsin VAX computer: we thank Sau Lan Wu for giving us time on it. One of us (M.T.) is grateful to T. Walsh for the frequent hospitality of the DESY theory group during the completion of this work.

References

1) K. Wilson: Phys. Rev. D10, 2445 (1974)

2) M. Creutz: Phys. Rev. Lett. 43, 553 (1979);
K. Wilson: Cargèse Lectures 1979;
M. Creutz, L. Jacobs and C. Rebbi: Phys. Rev. D20, 1915 (1979)

3) K. Binder: in Phase Transitions and Critical Phenomena Vol. 5b, Ed. by C. Domb, M.S. Green (Academic Press 1976);
K. Binder (Editor): Monte Carlo Methods in Statistical Physics (Springer-Verlag 1979)

4) H. Fritzsch, M. Gell-Mann and H. Leutwyler: Phys. Lett. 47B, 365 (1973)

5) H.D. Politzer: Phys. Rev. Lett. 30, 1346 (1973);
D. Gross and F. Wilczek: Phys. Rev. D9, 980 (1974);
S. Coleman, D. Gross: Phys. Rev. Lett. 31, 851 (1973)

6) M. Creutz: Phys. Rev. Lett. 45, 313 (1980);
Phys. Rev. D21, 2308 (1980)

7) K. Ishikawa, G. Schierholz and M. Teper: Phys. Lett. 110B, 399 (1982)

8) K. Ishikawa, G. Schierholz and M. Teper: Phys. Lett. 116B, 429 (1982)

9) K. Ishikawa, G. Schierholz and M. Teper: Zeitschrift für Physik C16, 69 (1982)

10) K. Ishikawa, A. Sato, G. Schierholz and M. Teper: Phys. Lett. 120B, 387 (1983)

11) K. Ishikawa, A. Sato, G. Schierholz and M. Teper: in preparation

12) J. Kogut, D. Sinclair and L. Susskind: Nuclear Physics 114B, 199 (1976)

13) G. Münster: Nuclear Physics B190, 439 (1981), B200, 536 (1982);
Bern preprint BUTP-21 (1982);
J. Smit: Amsterdam preprint ITFA-82-3 (1982)

14) B. Berg: Phys. Lett. 97B, 401 (1980);
G. Bhanot and C. Rebbi: Nuclear Physics B180, 469 (1981)

15) M. Falcioni, E. Marinari, M.L. Paciello, G. Parisi, F. Rapuano,
B. Taglienti and Zhang Yi-cheng: Phys. Letters 110B, 295 (1982)

16) B. Berg, A. Billoire and C. Rebbi: Annals Phys. 142, 185 (1982)

17) B. Berg and A. Billoire: Phys. Lett. 113B, 65 (1982); 114B, 324 (1982)

18) J. Engels, F. Karsch, H. Satz and I. Montvay:
Phys. Lett. 102B, 332 (1981); Bielefeld preprint BI-TP-29 (1981)

19) C. Michael and I. Teasdale: Liverpool Preprint LTH 96 (1982)

20) M. Falcioni, E. Marinari, M.L. Paciello, G. Parisi, F. Rapuano,
B. Taglienti and Zhang Yi-cheng: Rome preprint (1982)

21) K.H. Mütter and K. Schilling: CERN preprint TH 3246 (1982);
Wuppertal preprint WU B 82-14 (1982)

22) C.E. Carlson, T.H. Hansson and C. Peterson: MIT preprint CTP # 1020 (1982);
T.H. Hansson, K. Johnson and C. Peterson: Phys. Rev. D26, 2069 (1982) and
references therein

23) R.P. Feynman: Rev. Mod. Phys. 20, 267 (1948);
R.P. Feynman and A.R. Hibbs: Quantum Mechanics and Path Integrals
(McGraw-Hill 1965)

24) G. 't Hooft and M. Veltman: Diagrammar, CERN report CERN 73-9 (1973)

25) For a discussion of the relationship between a field theory and a
statistical mechanical system see:
K.G. Wilson and J. Kogut: Physics Reports 12C (1974)

26) M. Lüscher: Comm. Math. Phys. 54, 283 (1977);
K. Osterwalder and E. Seiler: Ann. Phys. 110, 440 (1978)

27) M. Creutz: Phys. Rev. D21, 2308 (1980);
E. Pietarinen: Nucl. Phys. B190, 349 (1981)

28) K.G. Wilson: closing remarks at the Abingdon Lattice Meeting (March 1981)

29) L. McLerran and B. Svetitsky: Phys. Lett. 98B, 195 (1981) and
Phys. Rev. D24, 450 (1981);
J. Kuti, J. Polonyi and K. Szlachanyi: Phys. Lett. 98B, 199 (1981);
J. Engels, F. Karsch, H. Satz and I. Montvay: Phys. Lett. 101B, 89 (1981);
K. Kajantie, C. Montonen and E. Pietarinen: Zeitschrift für Physik C9,
253 (1981):
I. Montvay and E. Pietarinen: DESY preprint DESY 81-077 (1981)

30) F. James: Monte Carlo Theory and Practice, CERN preprint DD/80/6 (1980)

31) D.R.T. Jones: Nuclear Physics B75, 531 (1974);
W.E. Caswell: Phys. Rev. Lett. 33, 244 (1974)

32) A. Hasenfratz and P. Hasenfratz: Nuclear Physics B193, 210 (1981)
and references therein

33) M.A. Shifman, A.I. Vainshtein and V.I.I. Zakharov: Nuclear Physics B147,
385, 519 (1979)

34) K. Ishikawa, G. Schierholz, H. Schneider and M. Teper: DESY preprint
DESY 82-087 / LAPP-TH 70 (1982); and references therein

35) E. Witten: Nuclear Physics B156, 269 (1979)

36) P. DiVecchia: Schladming lectures (1980); and references therein

37) P. DiVecchia, K. Fabricius, G.G. Rossi and G. Veneziano: Nuclear Physics B192, 392 (1981); CERN preprint TH 3180 (1981);
K. Ishikawa, G. Schierholz, H. Schneider and G. Schierholz: in preparation

38) D.L. Scharre et al.: Phys. Lett. 97B, 329 (1980);
C. Edwards et al.: Phys. Rev. Lett. 48, 458 (1982); 49, 259 (1982);
For theoretical comments see:
K. Ishikawa: Phys. Rev. Lett. 46, 978 (1981);
M. Chanowitz: Phys. Rev. Lett. 46, 981 (1981);
For a recent review see:
E.D. Bloom: SLAC preprint SLAC-PUB-2976 (1982)

39) R. Brower, M. Nauenberg and T. Schalk: Phys. Rev. D24, 548 (1981)

40) C.B. Lang and C. Rebbi: Phys. Letters 115B, 137 (1982)

41) K. Ishikawa, G. Schierholz, H. Schneider and M. Teper: ref.(34);
and in preparation

42) B. Lautrup and M. Nauenberg: Phys. Rev. Letters 45 (1980) 1755

43) P. DiVecchia, K. Fabricius, G.C. Rossi and G. Veneziano: ref.(37)

44) F. Karsch: Nuclear Physics B205, 285 (1982)

Table Captions

Tab. 1: The average action of various sublattices centred within a 10^4 lattice with antiperiodic boundary conditions and the value on an 8^4 lattice with periodic boundary conditions.

Tab. 2: Values of Γ_A / Γ_0 for $\vec{p} = 0$ 0^+, 2^+, 2^- wave-functionals based on the operators in Fig. 7 (a-h) on a $4^3 \cdot 8$ lattice at $\beta = 2.3$.

Tab. 3: As in Tab. 2 for 1^+, 1^- and 3^+.

Tab. 4: Parallel plaquette correlation functions.

Tab. 5: 0^+, 2^+ correlation functions on a $5^3 \cdot 40$ lattice.

Tab. 6: As Tab. 5 but for 0^-.

Tab. 7: Comparison of 0^+ and 2^+ correlation functions on a $5^3 \cdot 40$ and $4^3 \cdot 8$ lattice.

Tab. 1

lattice	action
4^4	0.4386 ± 0.002
6^4	0.4830 ± 0.001
8^4	0.5108 ± 0.004
10^4	0.5225 ± 0.001
8^4 with periodic b.c.	0.6019 ± 0.0003

Tab. 2

loop	Γ_a / Γ_0		
	0^+	2^+	2^-
(a)	0.121 ± 0.003	0.0295 ± 0.0015	-
(b)	0.154 ± 0.004	0.039 ± 0.002	-
(c)	0.158 ± 0.003	0.0444 ± 0.0017	-
(d)	-	0.027 ± 0.002	-
(e)	-	0.016 ± 0.002	-
(f)	0.113 ± 0.006	0.019 ± 0.003	0.015 ± 0.002
(g)	0.122 ± 0.006	0.020 ± 0.002	0.015 ± 0.002
(h)	0.168 ± 0.003	0.022 ± 0.002	0.020 ± 0.002

Tab. 3

loop	Γ_a / Γ_0		
	1^+	1^-	3^+
(d)	-	-	0.012 ± 0.002
(e)	-	-	0.011 ± 0.002
(f)	0.007 ± 0.001	0.013 ± 0.001	-
(g)	0.0025 ± 0.001	0.008 ± 0.001	-
(h)	0.0025 ± 0.001	0.002 ± 0.001	-

Tab. 4

n	$\Gamma_{na} / \Gamma_{(n-1)a}$			
	$5^3 \cdot 40$		$4^3 \cdot 8$	
	time	space	time	space
1	0.341 ± 0.001	0.134 ± 0.004	0.0302 ± 0.0005	0.0316 ± 0.0005
2	0.367 ± 0.002	0.084 ± 0.028	0.045 ± 0.01	0.057 ± 0.03
	0.390 ± 0.002			
4	0.412 ± 0.002			
5	0.434 ± 0.003			
6	0.42 ± 0.02			
7	0.47 ± 0.05			
8	0.51 ± 0.04			

Tab. 5

n	Γ_{na_t} / Γ_o	
	0^+	2^+
1	0.416 ± 0.004	0.314 ± 0.0013
2	0.230 ± 0.003	0.125 ± 0.0007
3	0.146 ± 0.004	0.0566 ± 0.0008
4	0.099 ± 0.003	0.0278 ± 0.0006
5	0.070 ± 0.003	0.0145 ± 0.0015
6	0.052 ± 0.003	0.0082 ± 0.0009
7	0.038 ± 0.002	0.0046 ± 0.0008
8	0.028 ± 0.002	0.0024 ± 0.0008
9	0.019 ± 0.002	0.0012 ± 0.0009
10	0.013 ± 0.002	0.0011 ± 0.0009
11	0.008 ± 0.002	0.0015 ± 0.0011
12	0.004 ± 0.003	0.0009 ± 0.0022

Tab. 6

n	Γ_{na_t} / Γ_o		
	FFD	FFDU	FFU
2	0.055 ± 0.003	0.20 ± 0.01	0.131 ± 0.006
4	0.013 ± 0.002	0.049 ± 0.006	0.041 ± 0.005
6	0.0012 ± 0.0014	0.018 ± 0.005	–
8	–	0.012 ± 0.008	–

Tab. 7

J^P	r	Γ_{2a}/Γ_a $5^3\cdot 40$	$4^3\cdot 8$	8^4	Γ_a/Γ_0 $5^3\cdot 40$	$4^3\cdot 8$	8^4
0^+	3.5	$0.31^{+}_{-}0.02$	$0.29^{+}_{-}0.03$	$0.32^{+0.07}_{-0.04}$	$0.120^{+}_{-}0.004$	$0.158^{+}_{-}0.002$	$0.122^{+}_{-}0.007$
	4.0	$0.28^{+}_{-}0.02$			$0.099^{+}_{-}0.002$		
2^+	3.5	$0.116^{+}_{-}0.02$	$0.11^{+}_{-}0.05$	$0.085^{+0.02}_{-0.005}$	$0.040^{+}_{-}0.001$	$0.044^{+}_{-}0.002$	$0.046^{+}_{-}0.005$
	4.0	$0.086^{+}_{-}0.02$			$0.028^{+}_{-}0.001$		

Figure Captions

Fig. 1: (a) A 2x2 loop of link matrices,
(b) a 0^+ combination of 2x2 loops,
(c) a 2^+ combination of 2x2 loops.

Fig. 2: A "2^+" combination of loops which is actually 0^+.

Fig. 3: The correlation length for measurements of the average action on the lattice for various β and two sequences of configurations.

Fig. 4: The variation of the upper error on the mass as we double the statistics.

Fig. 5: The average action on an L^4 sub-lattice of a 10^4 lattice with antiperiodic boundary conditions.

Fig. 6: Γ_a/Γ_0 for various operators versus the size of the operator in β = 2.3 lattice spacings.

Fig. 7: The diameter of the glueball R_G, the lattice spacing and half the lattice spatial extent versus β.

Fig. 8: Fluctuations of the average action on 8^4 lattices versus β.

Fig. 9: Loops used to form our wave-functionals.

Fig. 10: Γ_{2a}/Γ_a for a 0^+, $\vec{p} = 0$ wave-functional composed of 1x2 plaquettes for two sequences of configurations with differing starts.

Fig. 11: 0^+ and 2^+ glueball masses on an 8^4 lattice for various β.

Fig. 12: Γ_a/Γ_o for various operators on lattices of differing sizes.

Fig. 13: Ratio of energy to mass for our momentum smeared wavefunctions on an 8^4 lattice.

Fig. 14: The 0^+, $\vec{p} = 0$ correlation function on an asymmetric $5^3 \cdot 40$ lattice.

Fig. 15: The local slope of the 0^+ correlation function.

Fig. 16: The 2^+, $\vec{p} = 0$ correlation function on an asymmetric $5^3 \cdot 40$ lattice.

Fig. 17: The local slope of the 2^+ correlation function.

Fig. 18: 0^- correlation operators using two different $F\tilde{F}$ operators.

Fig. 19: A 0^- correlation function on the $5^3 \cdot 40$ lattice.

Fig. 20: A compilation of our results on the ratio of 2^+ to 0^+ masses.

Fig. 21: A compilation of our results on the ratio of 0^- to 0^+ masses.

Fig. 22: Correlation functions dominated by the two-0^+ glueball continuum:
(a,b) 0^+ partial wave,
(c,d) 2^+ partial wave.

Fig. 23: 0^+, 2^+ correlation functions in the high temperature, unconfined phase.

Fig. 24: The local slope of the 0^+ correlation function below and above the deconfining transition.

Fig. 25: The local slope of the 2^+ correlation function below and above the deconfining transition.

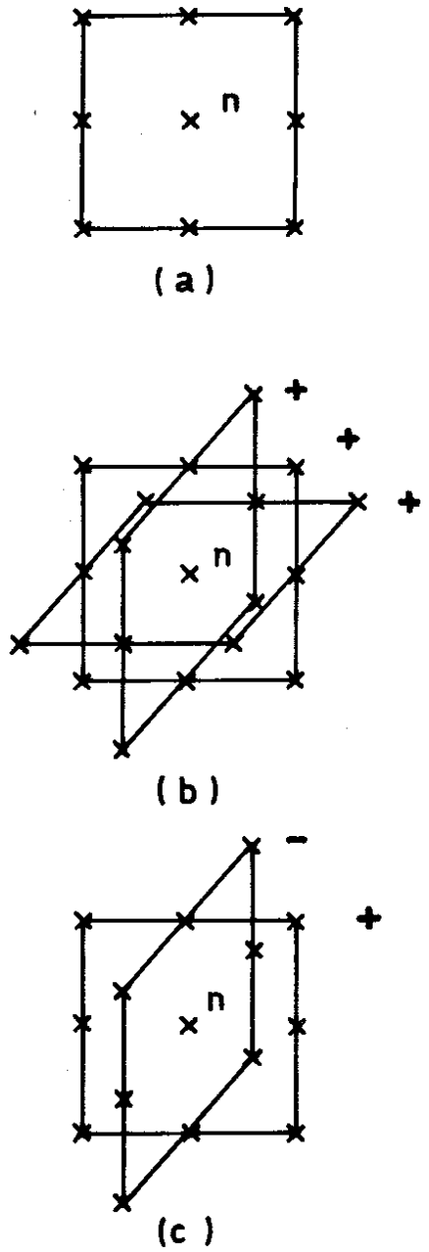

Fig.1

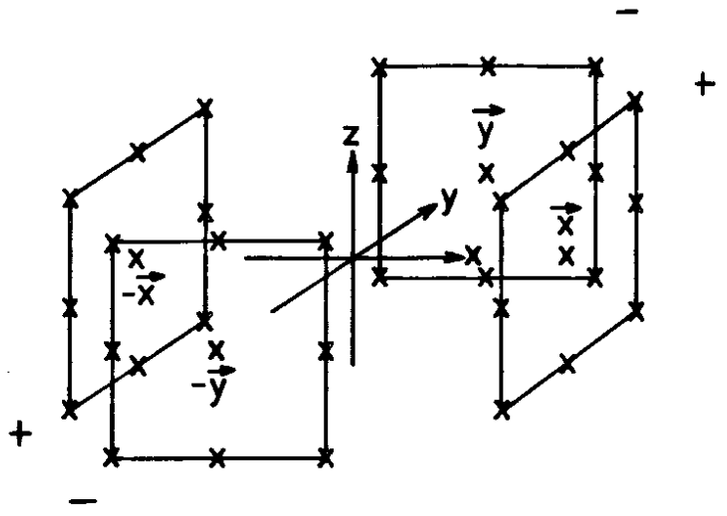

Fig. 2

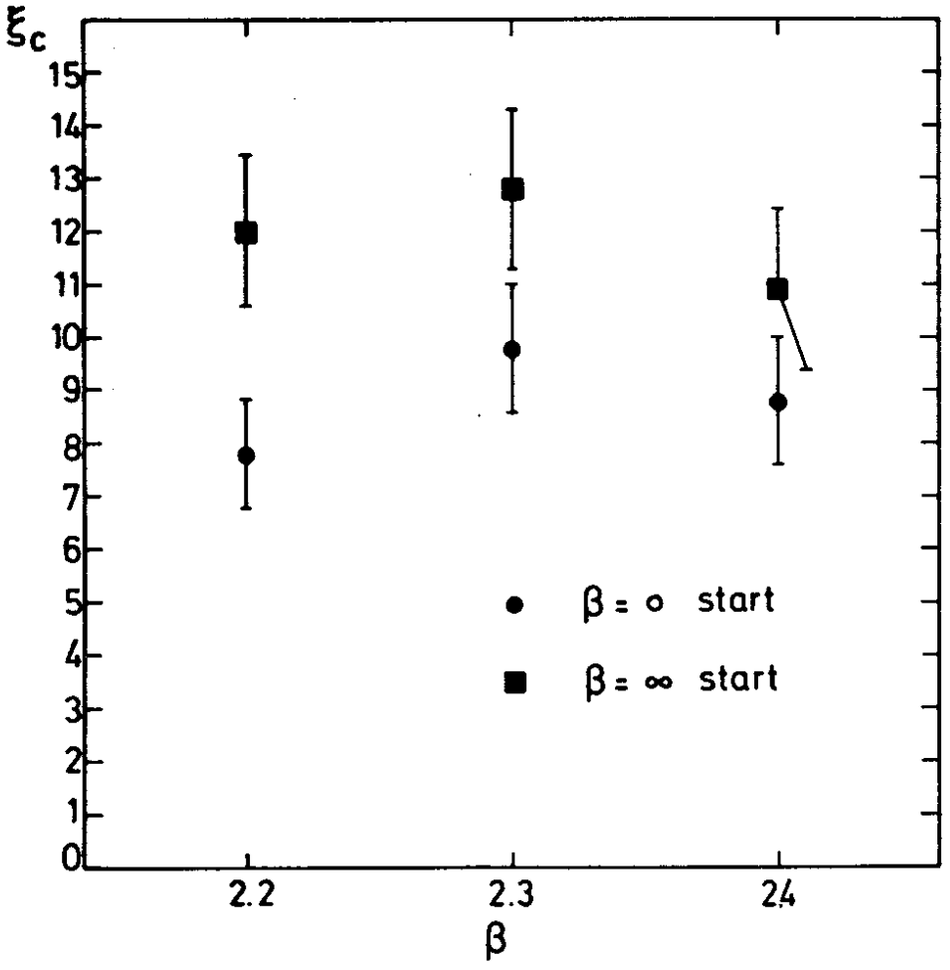
ξ_c
15
14
13
12
11
10
9
8
7
6
5
4
3
2
1
0
2.2
2.3
2.4
β
β = o start
β = ∞ start

Fig. 3

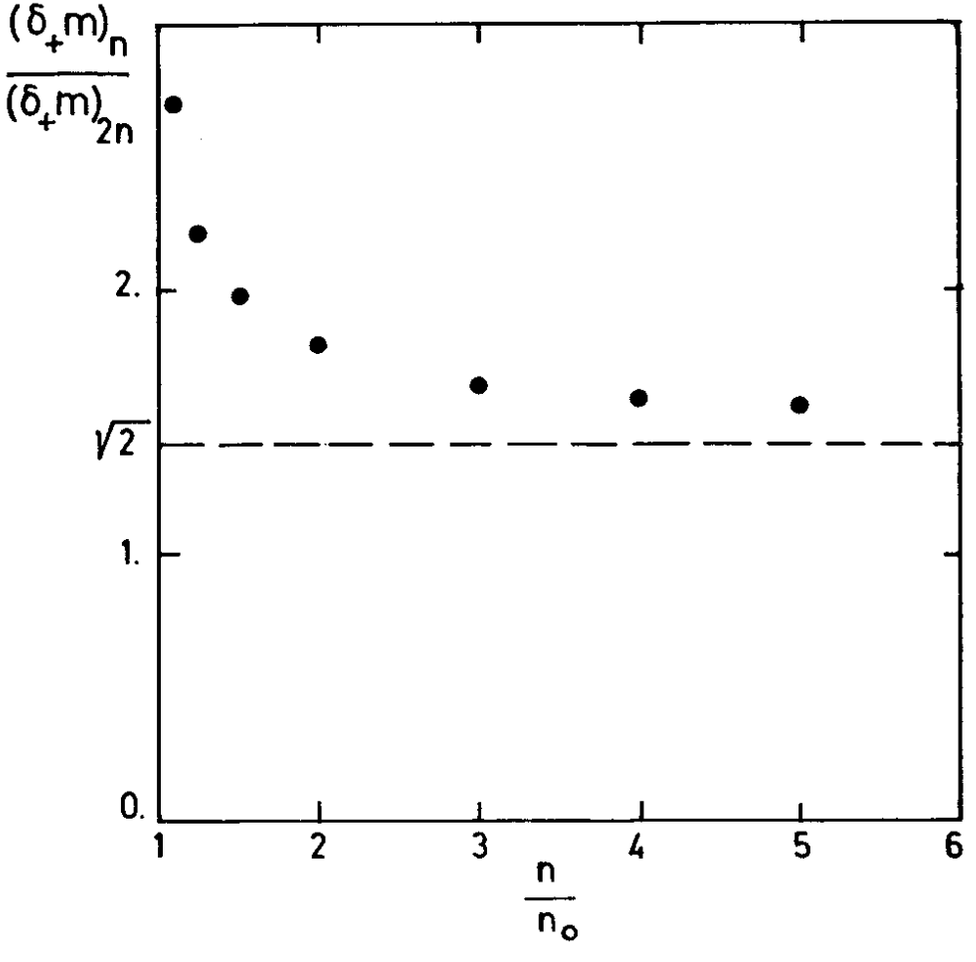
$\frac{(\delta_+ m)_n}{(\delta_+ m)_{2n}}$
2.
$\sqrt{2}$
1.
0.
1
2
3
4
5
6
$\frac{n}{n_o}$

Fig. 4

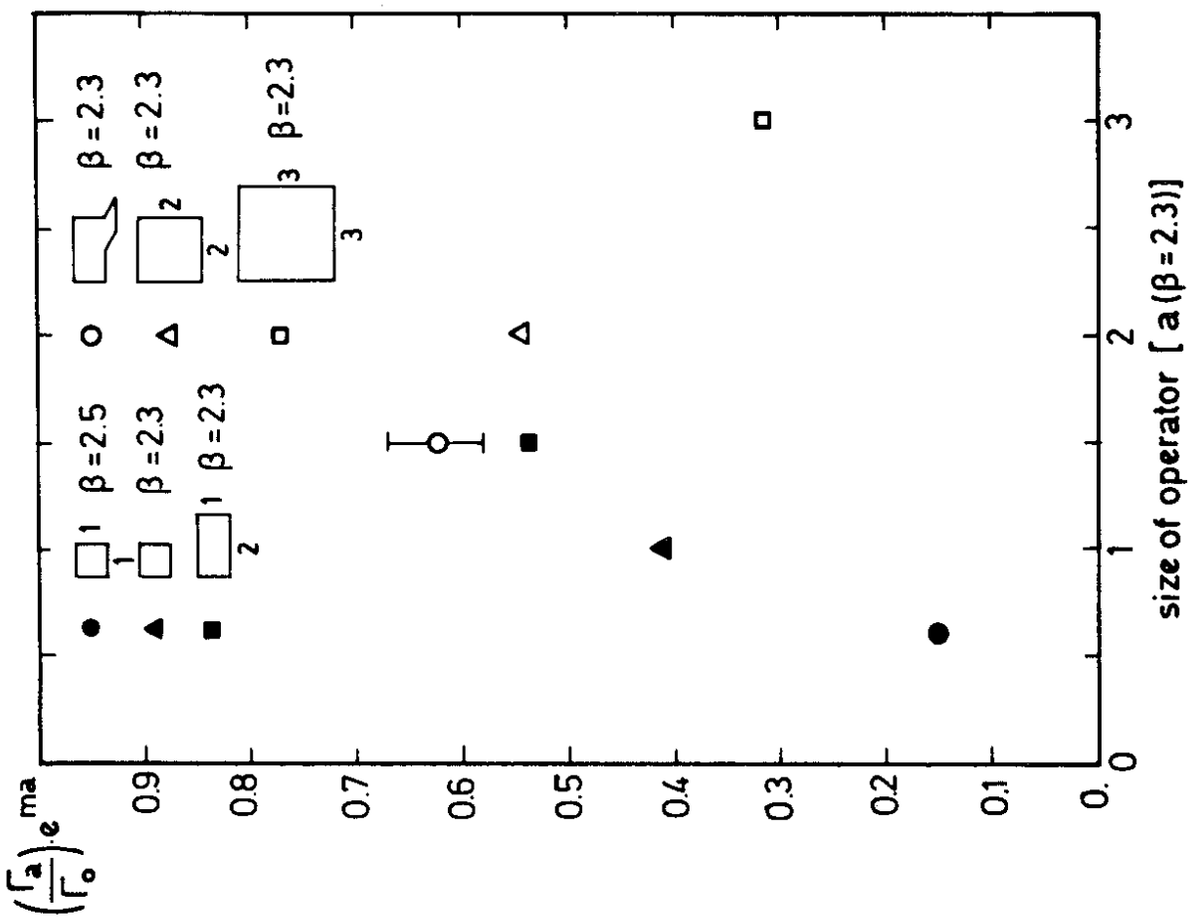
β=2.3
β=2.3
β=2.3
β=2.5
β=2.3
β=2.3
1
2
3
1
2
3
1
2
size of operator [a (β=2.3)]
0
1
2
3
0.9
0.8
0.7
0.6
0.5
0.4
0.3
0.2
0.1
0.
$\left(\frac{\Gamma_a}{\Gamma_0}\right)^{ma}$

Fig. 6

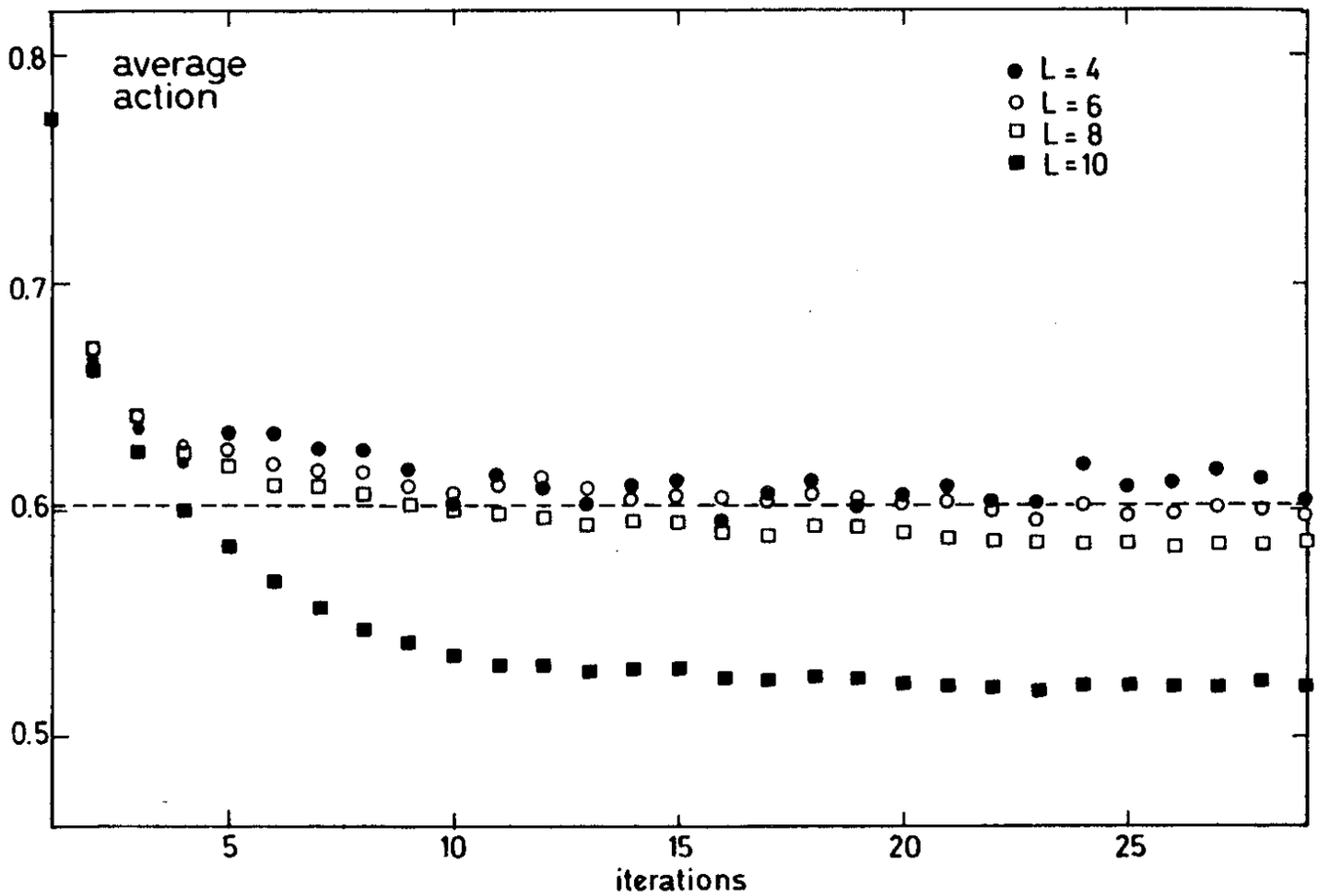
average
action
L = 4
L = 6
L = 8
L = 10
0.8
0.7
0.6
0.5
5
10
15
20
25
iterations

Fig. 5

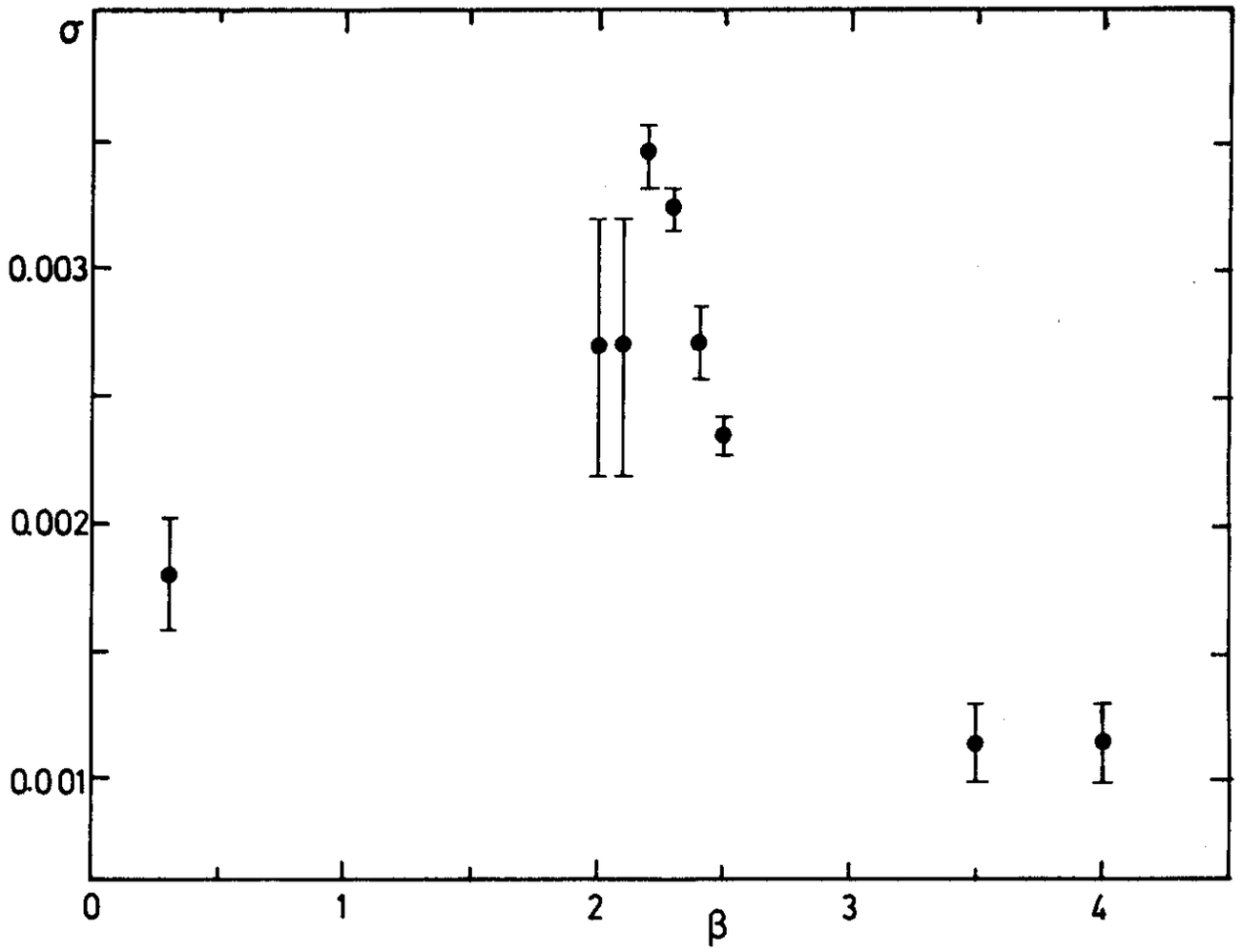
σ
0.003
0.002
0.001
0
1
2
3
4
β

Fig.8

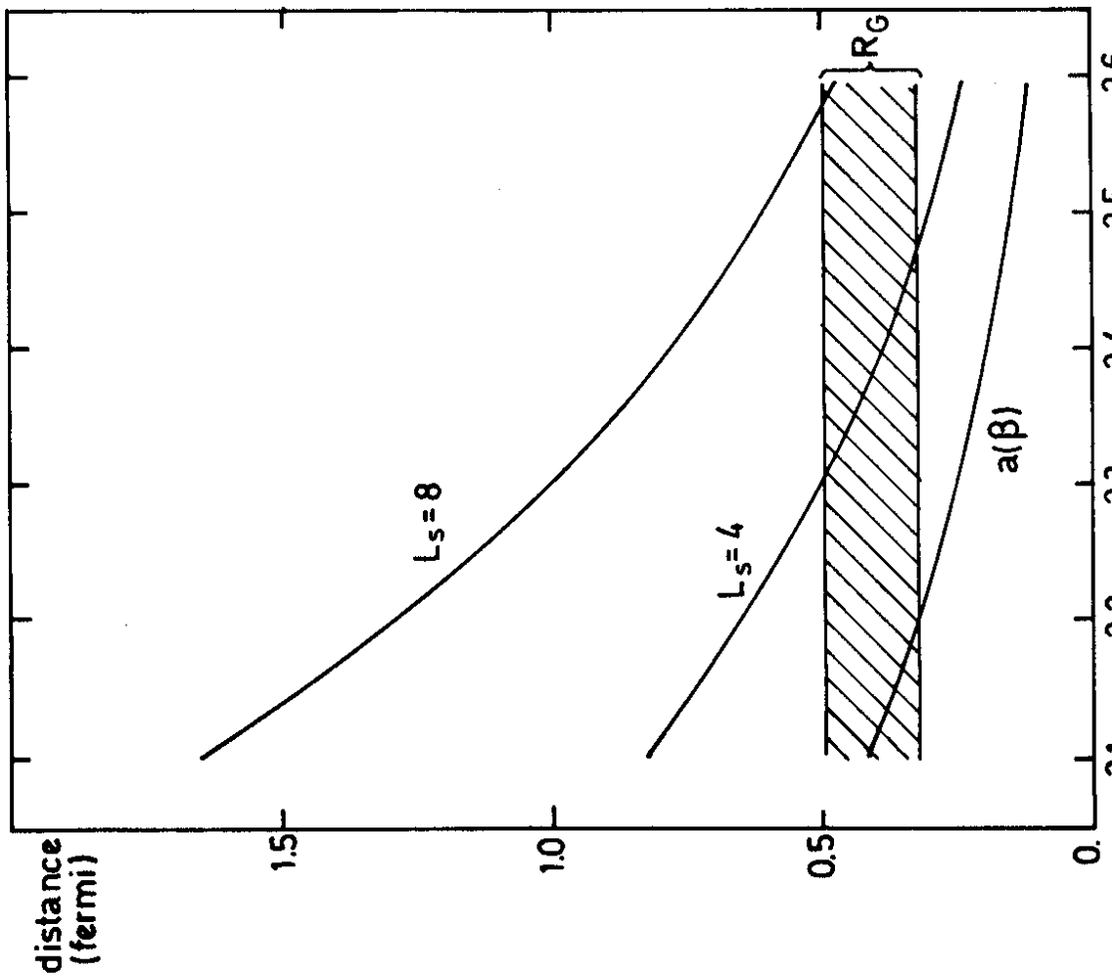
distance (fermi)
1.5
1.0
0.5
0.
$L_s=8$
$L_s=4$
R_G
a(β)
2.1
2.2
2.3
2.4
2.5
2.6
β

Fig.7

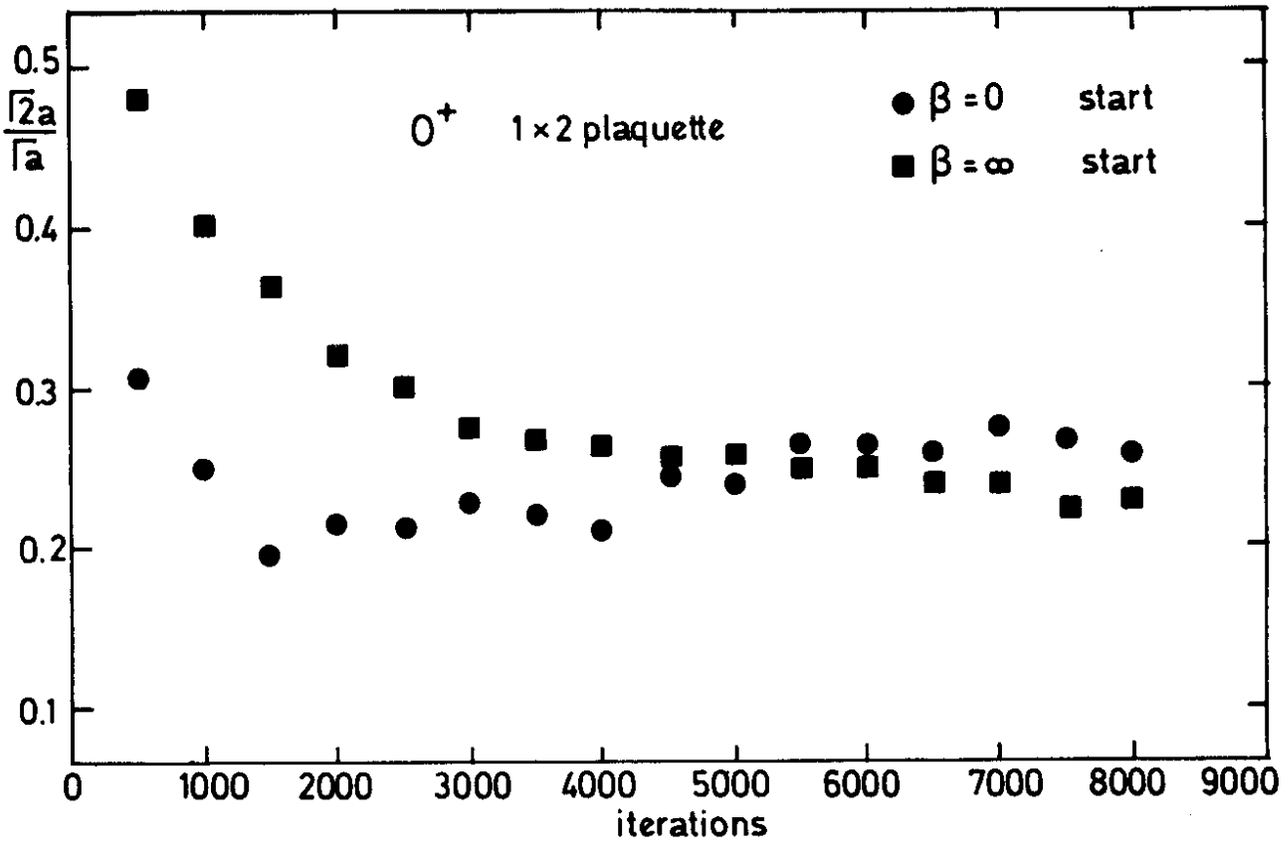
0.5
√2a/√a
0.4
0.3
0.2
0.1
0⁺ 1×2 plaquette
● β = 0 start
■ β = ∞ start
0
1000
2000
3000
4000
5000
6000
7000
8000
9000
iterations

Fig.10

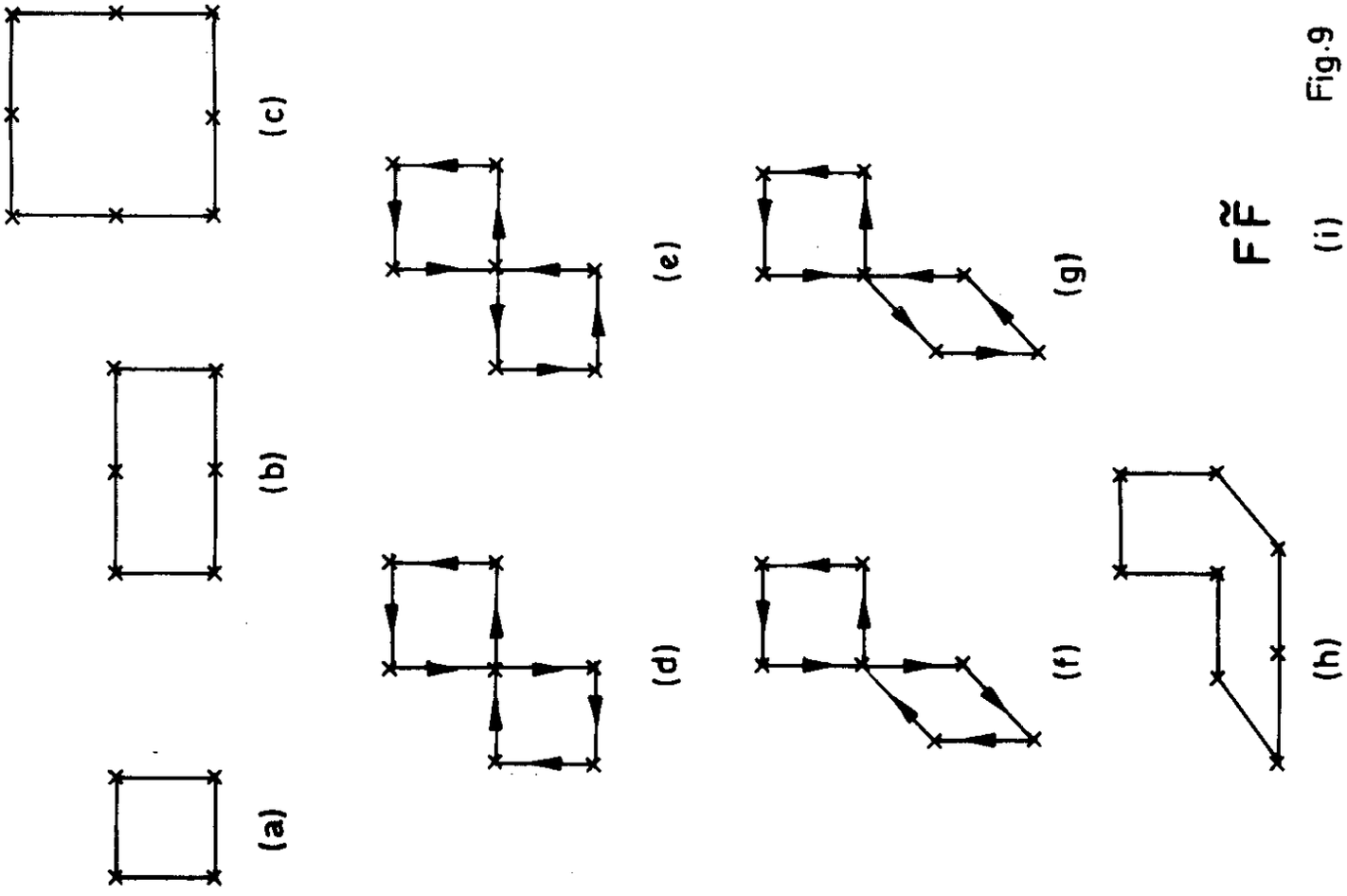
(a)
(b)
(c)
(d)
(e)
(f)
(g)
(h)
(i)

Fig.9

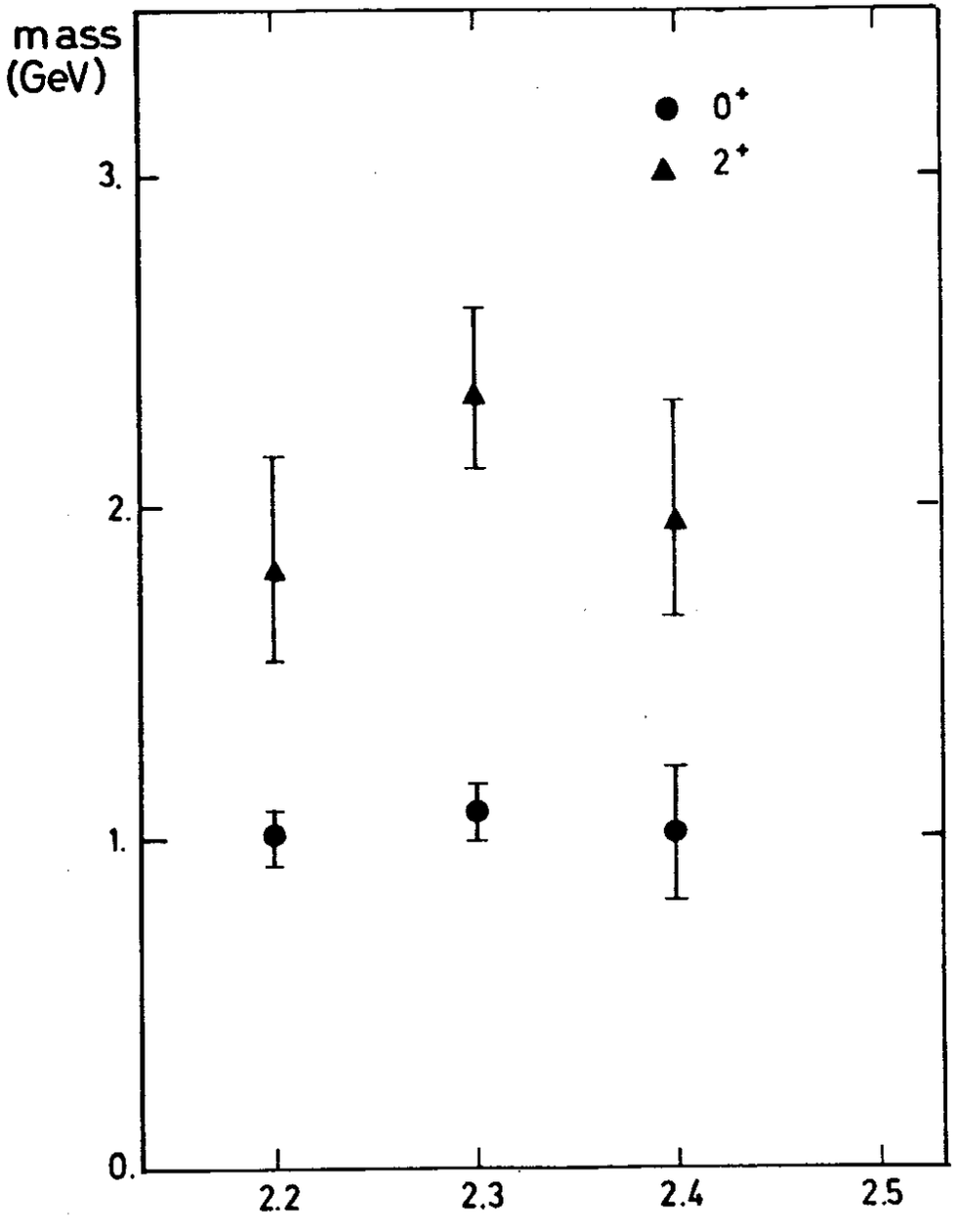
mass
(GeV)
3.
2.
1.
0.
2.2
2.3
2.4
2.5
0+
2+

Fig. 11

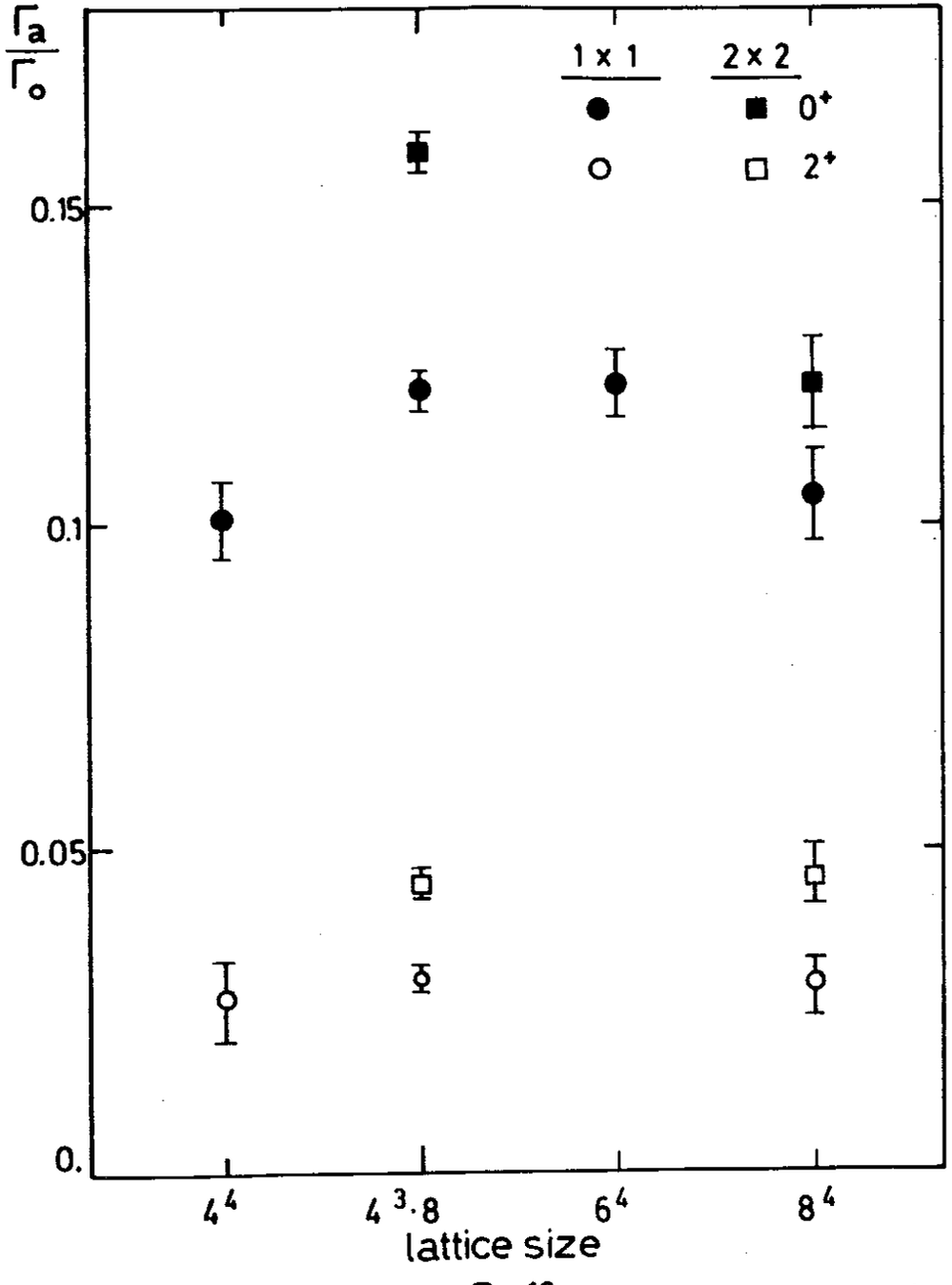
Γa/Γo
1 x 1
2 x 2
0+
2+
0.15
0.1
0.05
0.
4^4
4^3.8
6^4
8^4
lattice size

Fig. 12

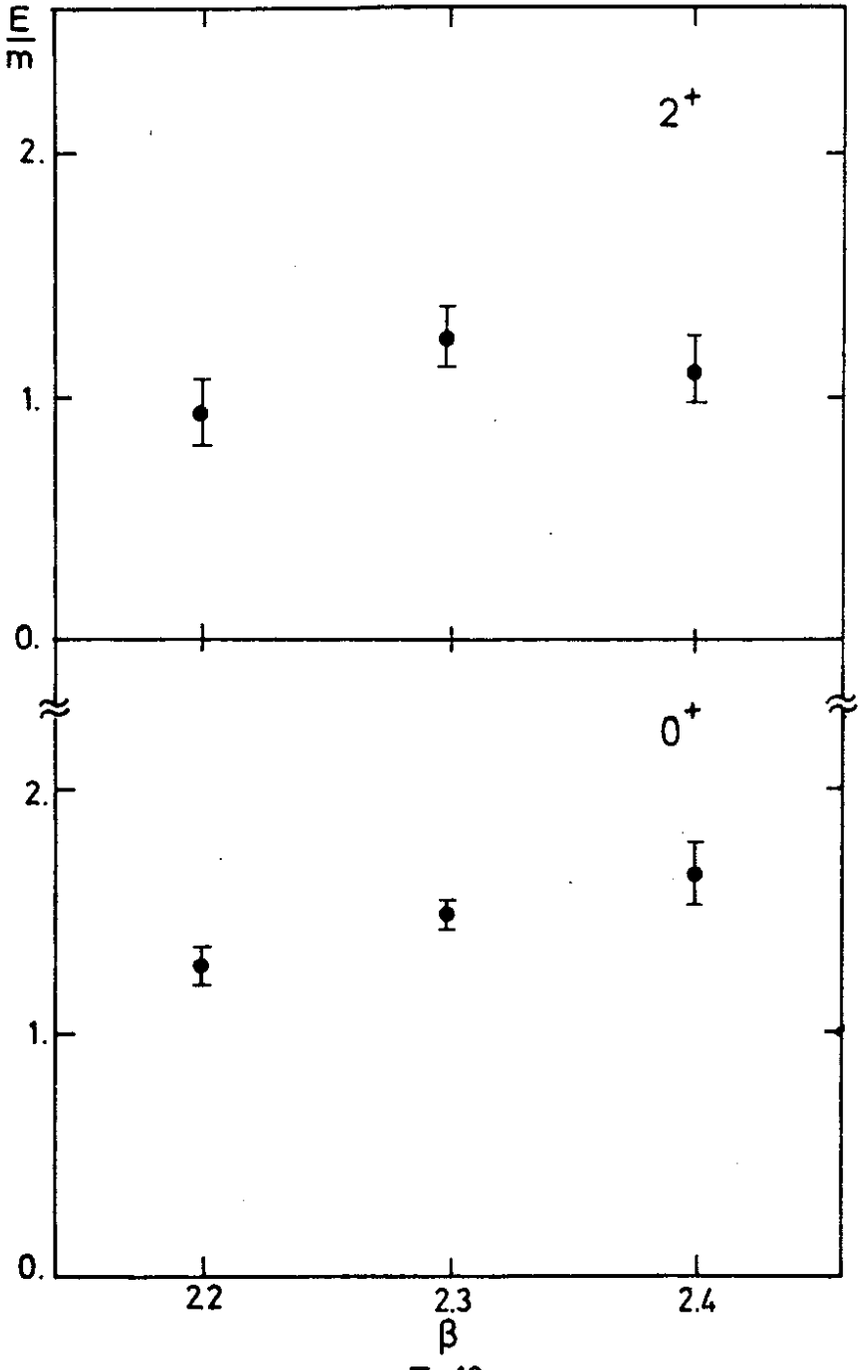
E/m
2.
1.
0.
2⁺
0⁺
2.
1.
0.
2.2
2.3
2.4
β

Fig.13

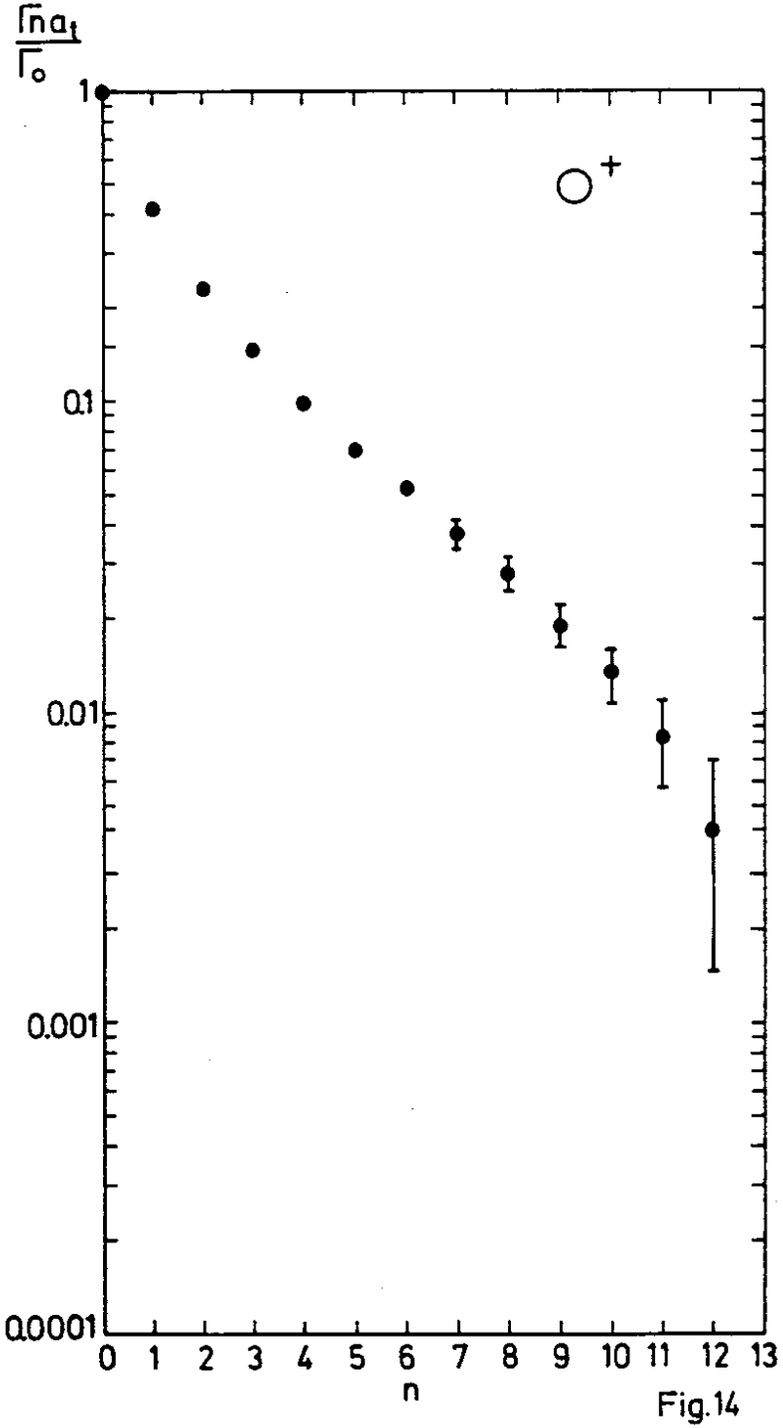
Γn a_t / Γ_o
1
0.1
0.01
0.001
0.0001
O⁺
0 1 2 3 4 5 6 7 8 9 10 11 12 13
n

Fig.14

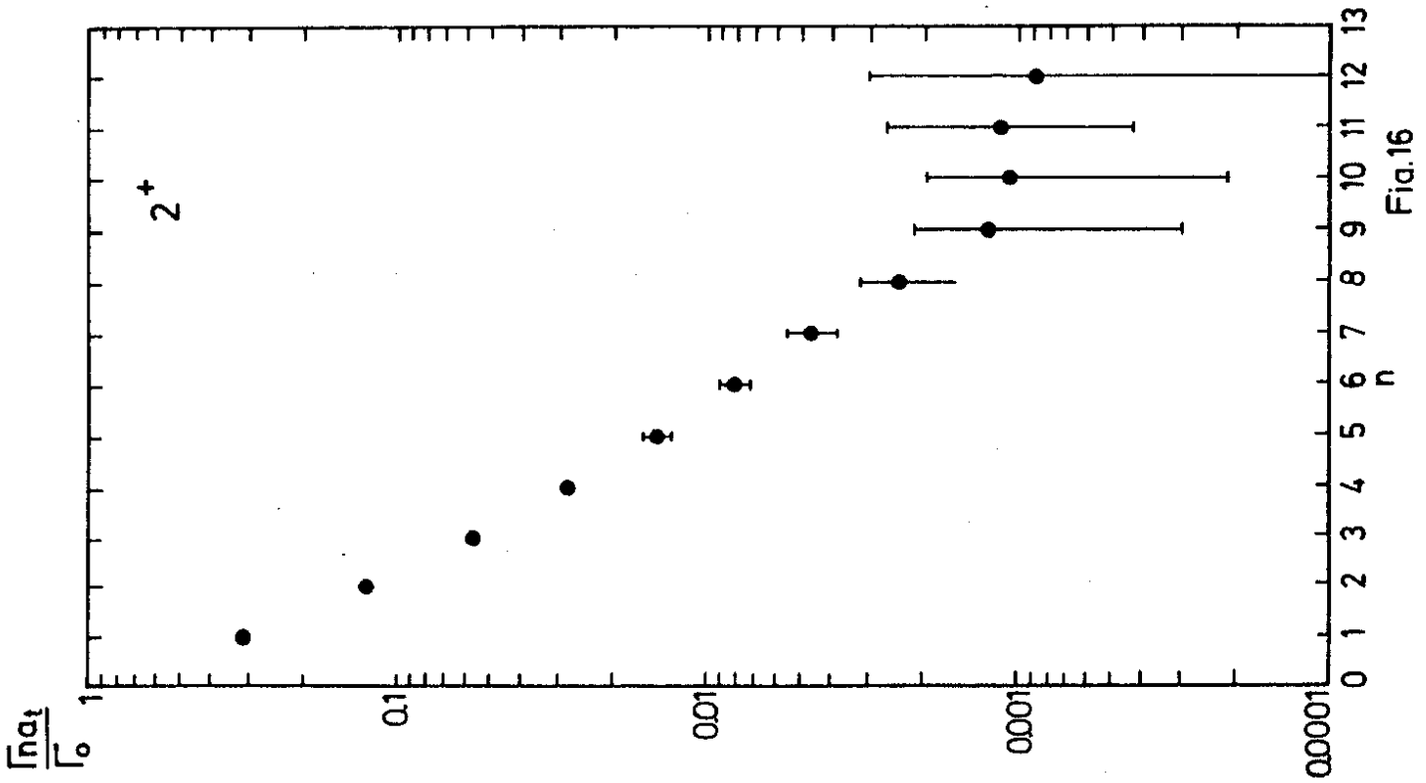
2+
Γn a t / Γo
1
0.1
0.01
0.001
0.0001
0 1 2 3 4 5 6 7 8 9 10 11 12 13
n

Fig.16

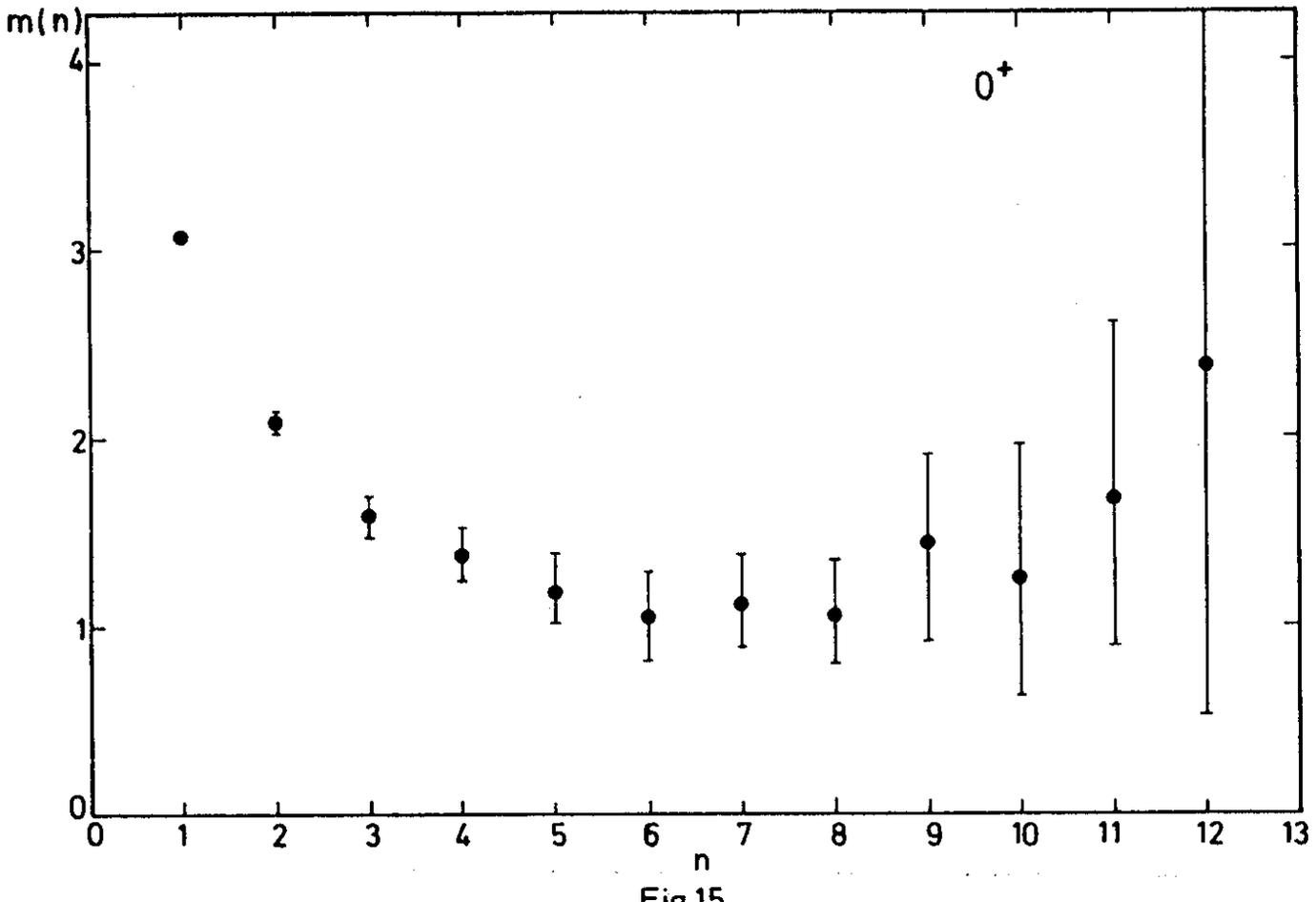
m(n)
0+
0 1 2 3 4
0 1 2 3 4 5 6 7 8 9 10 11 12 13
n

Fig.15

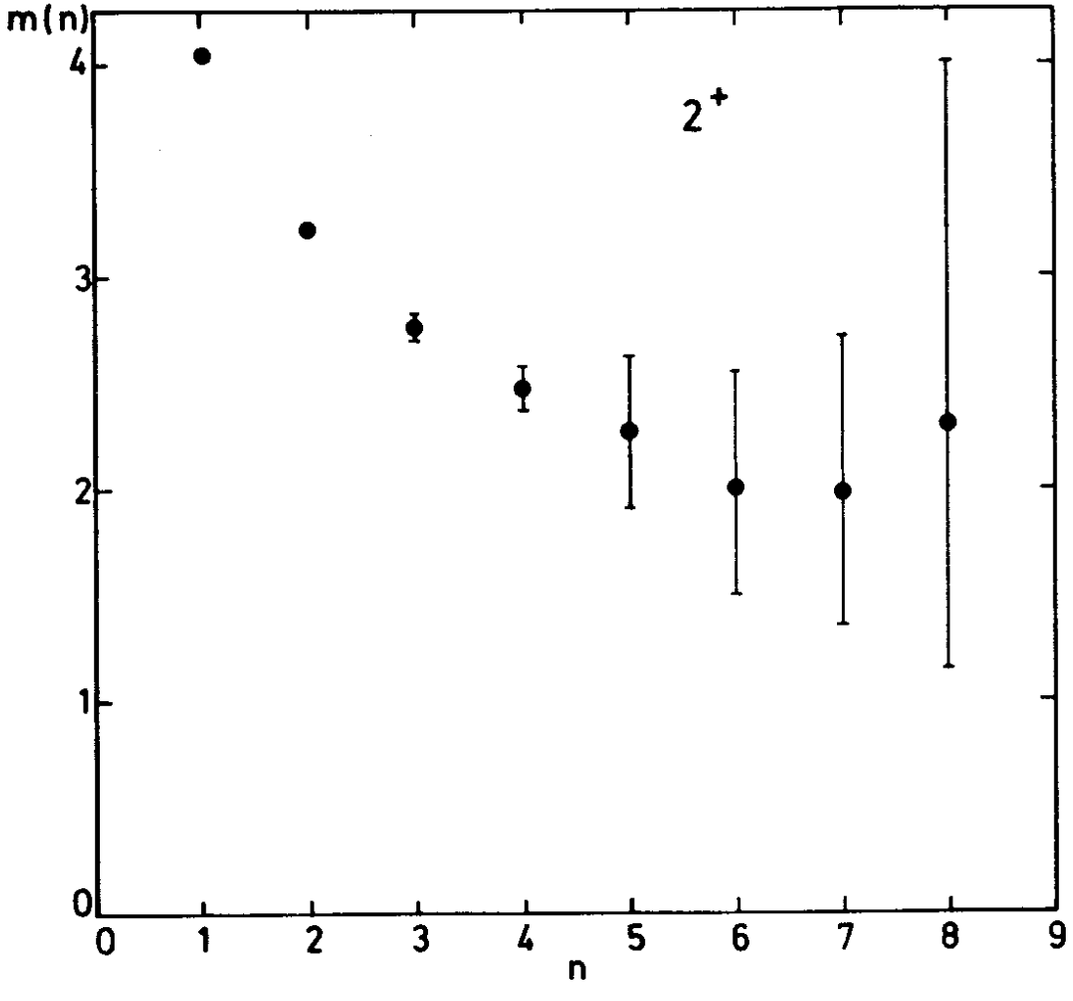

Fig.17

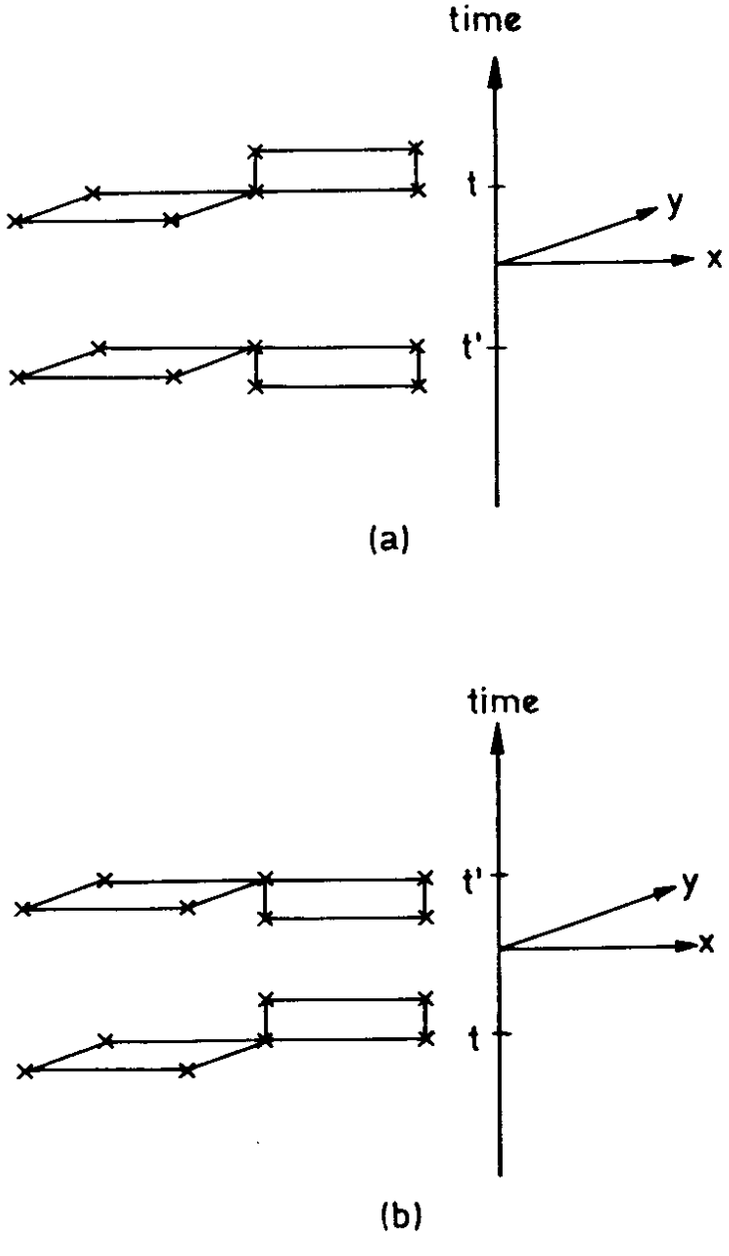

Fig. 18

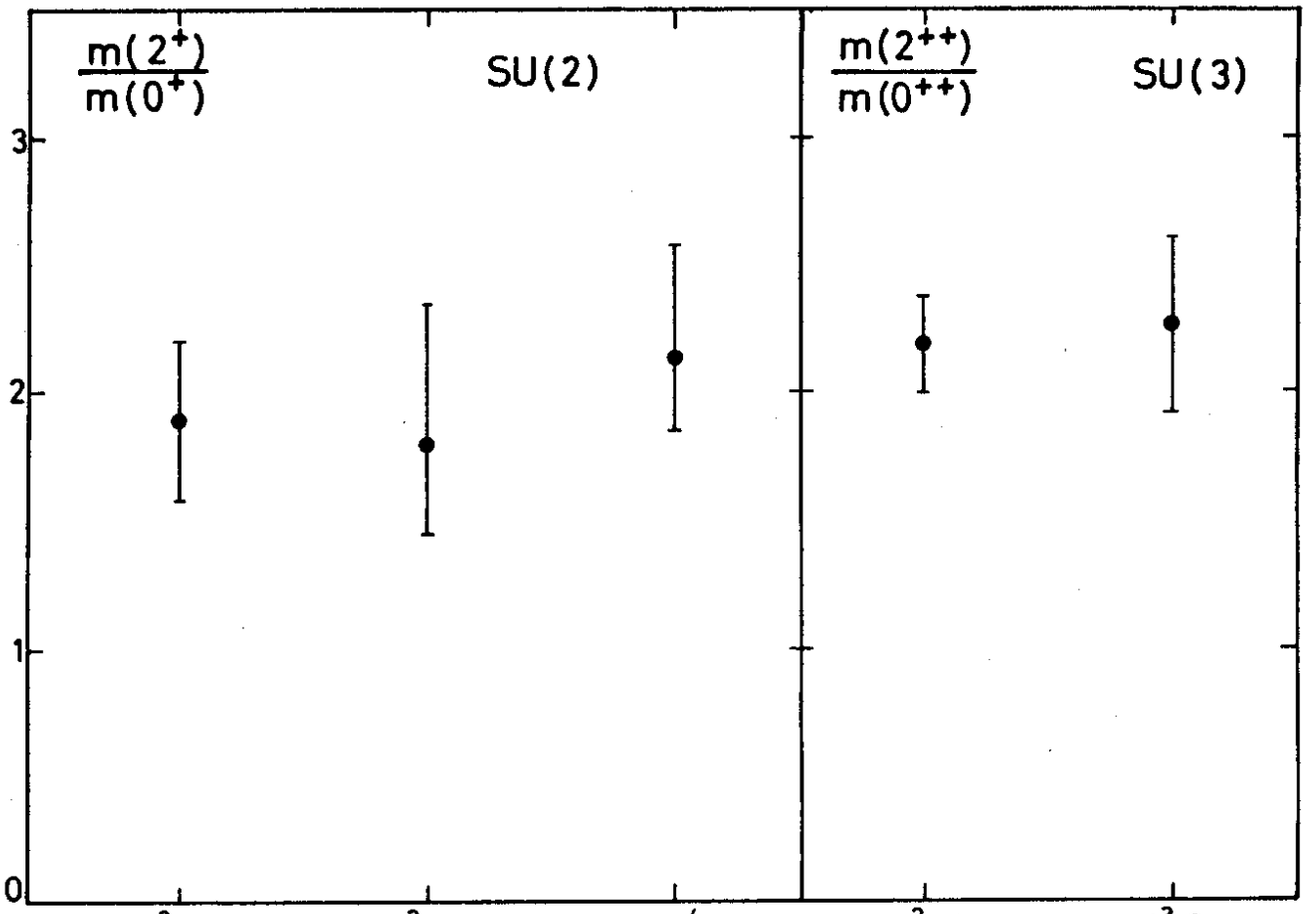
m(2+)/m(0+)
SU(2)
m(2++)/m(0++)
SU(3)
3
2
1
0
5³.40
4³.8
8⁴
4³.16
4³.8
lattice size
Fig. 20

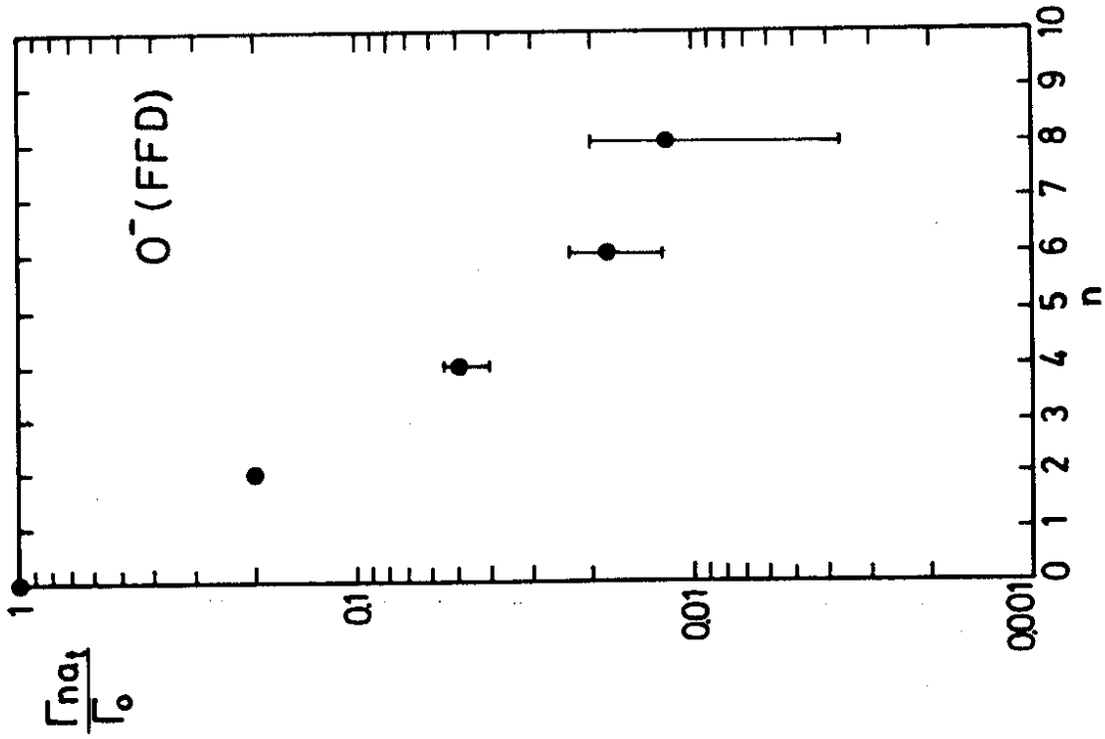
0⁻(FFD)
1
0.1
0.01
0.001
Γna/Γo
0 1 2 3 4 5 6 7 8 9 10
n
Fig.19

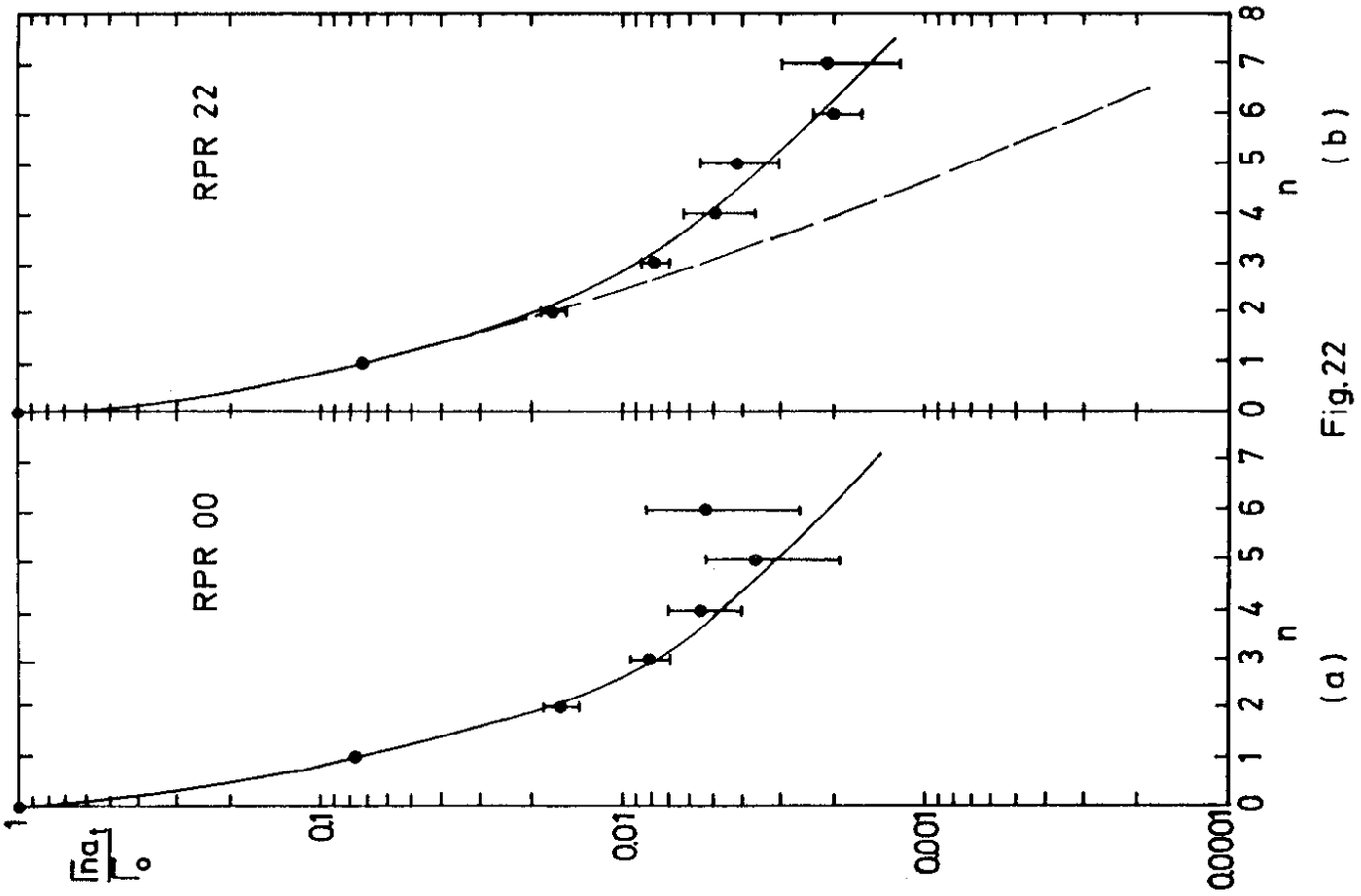
RPR 22
RPR 00
n
(b)
(a)
1
0.1
0.01
0.001
0.0001
0 1 2 3 4 5 6 7 8

Fig.22

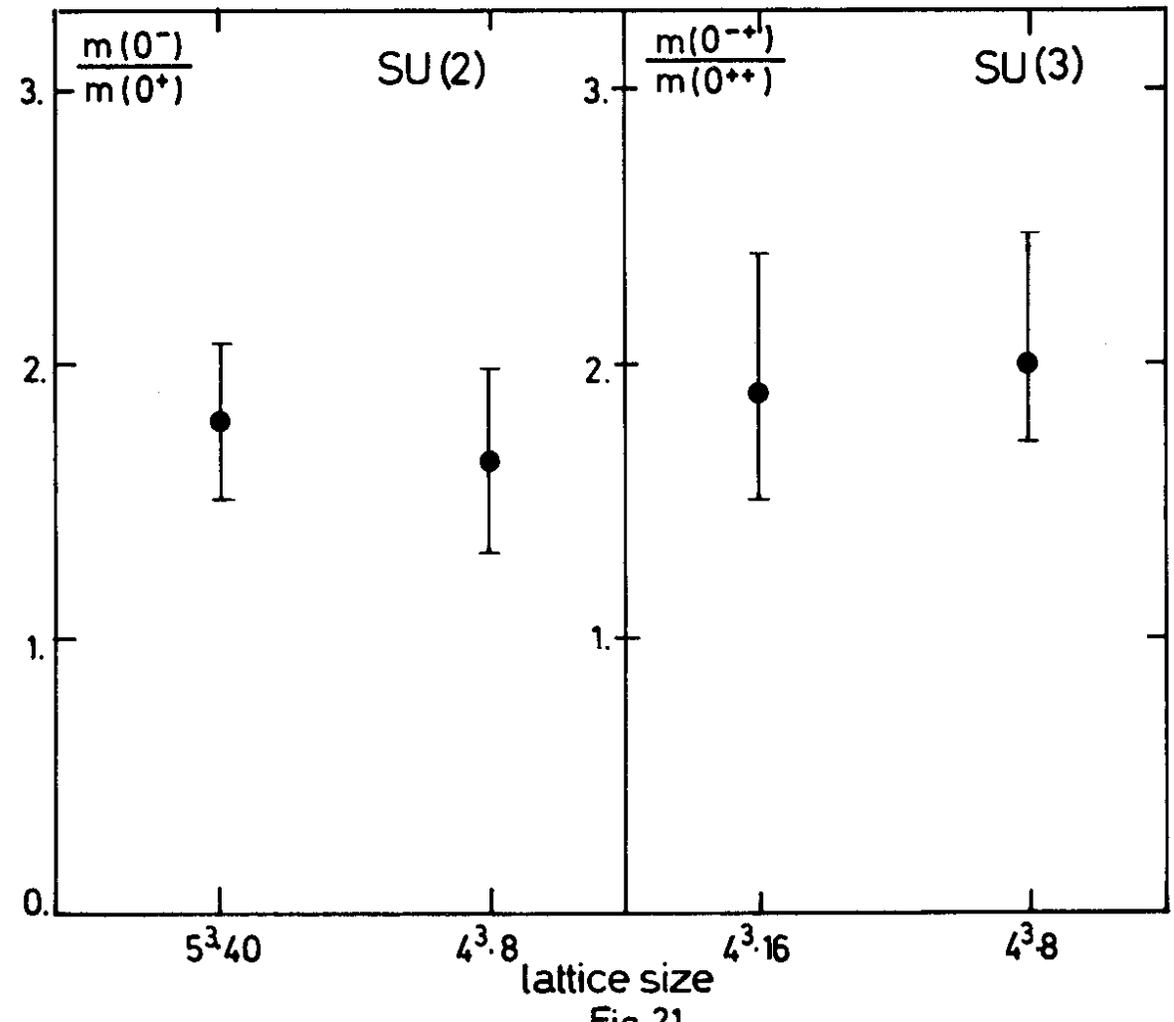
m(0⁻)/m(0⁺)
SU(2)
m(0⁻⁺)/m(0⁺⁺)
SU(3)
3.
2.
1.
0.
5³40
4³.8
4³.16
4³.8
lattice size

Fig.21

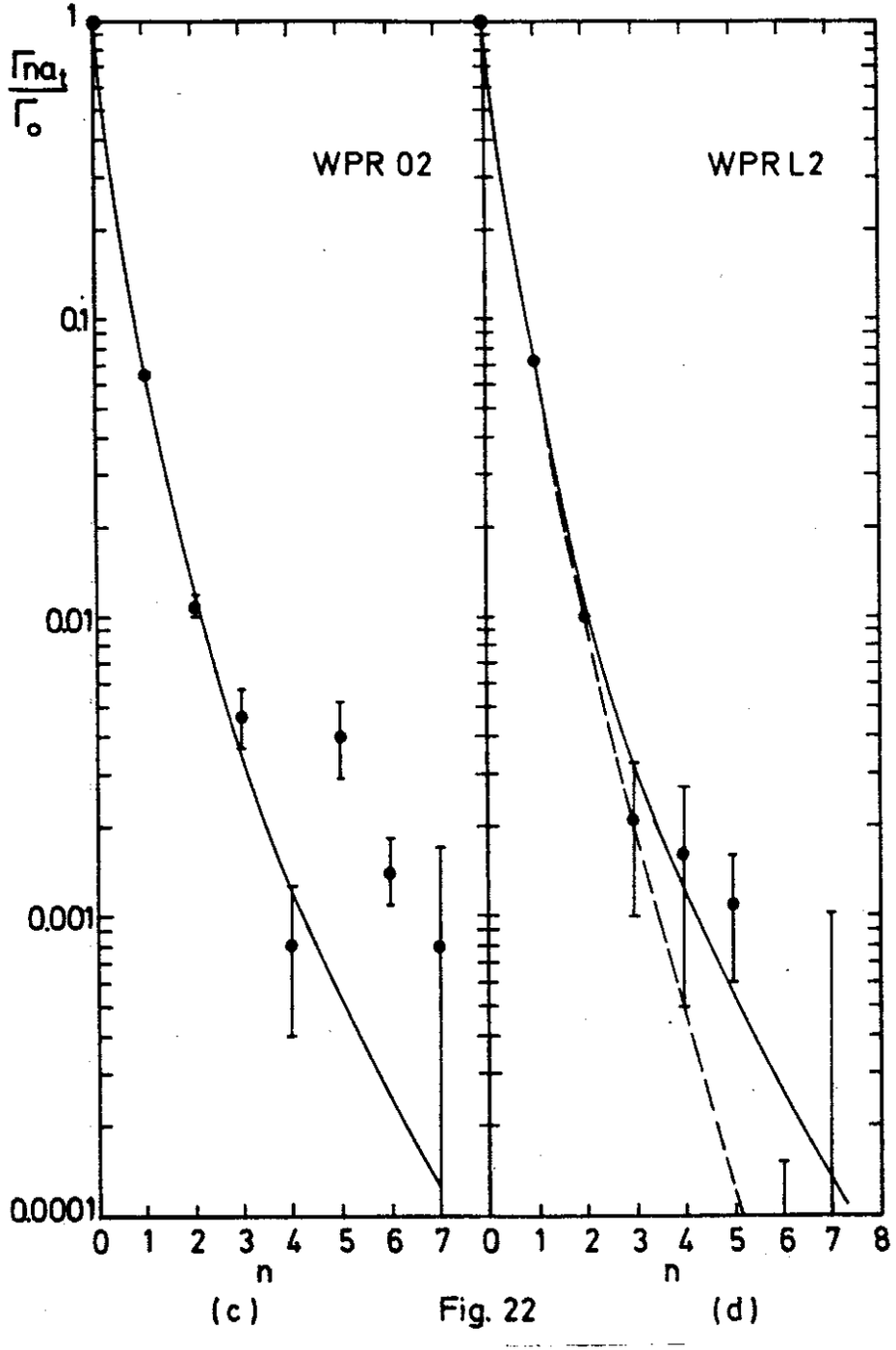

(c) Fig. 22 (d)

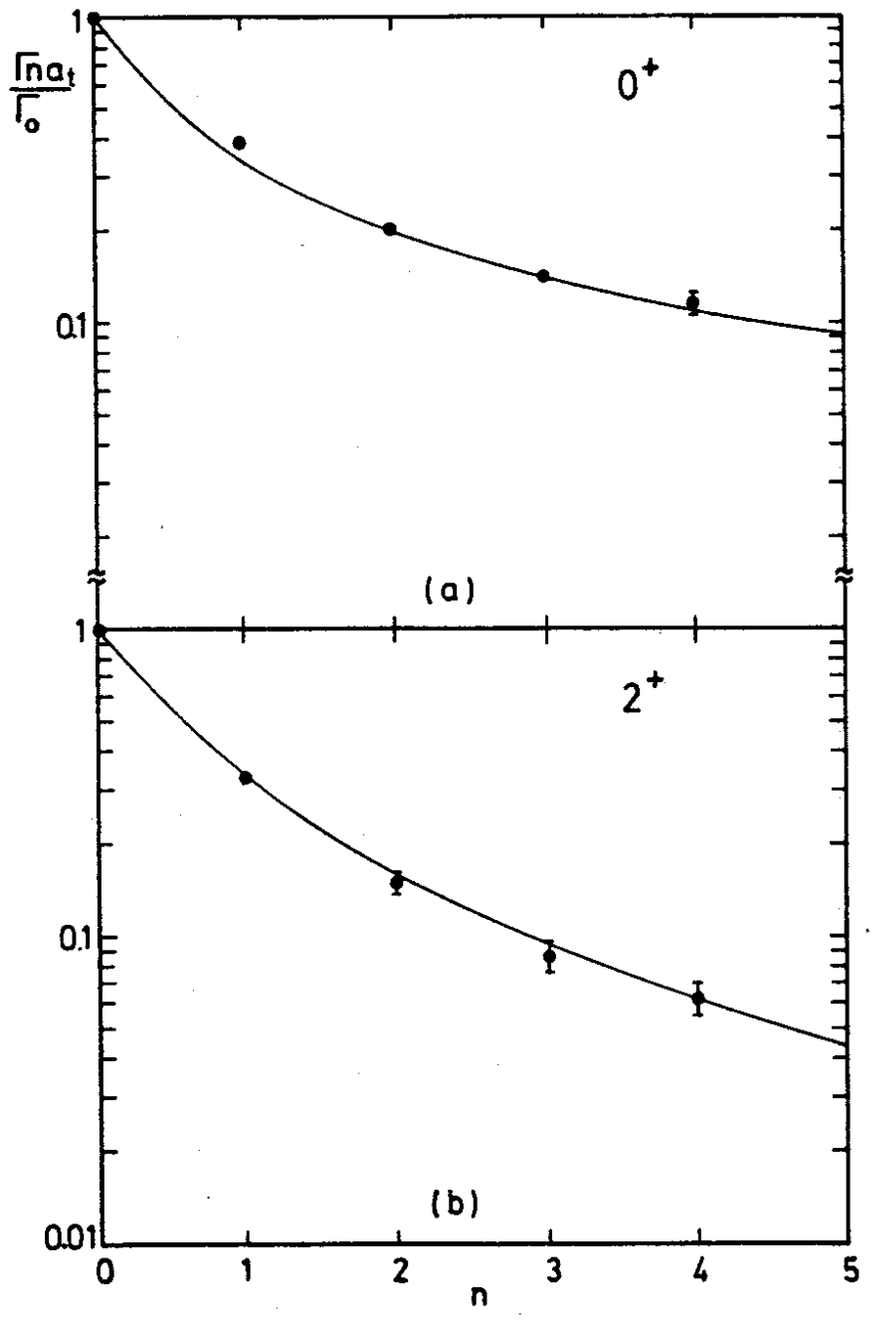

Fig. 23

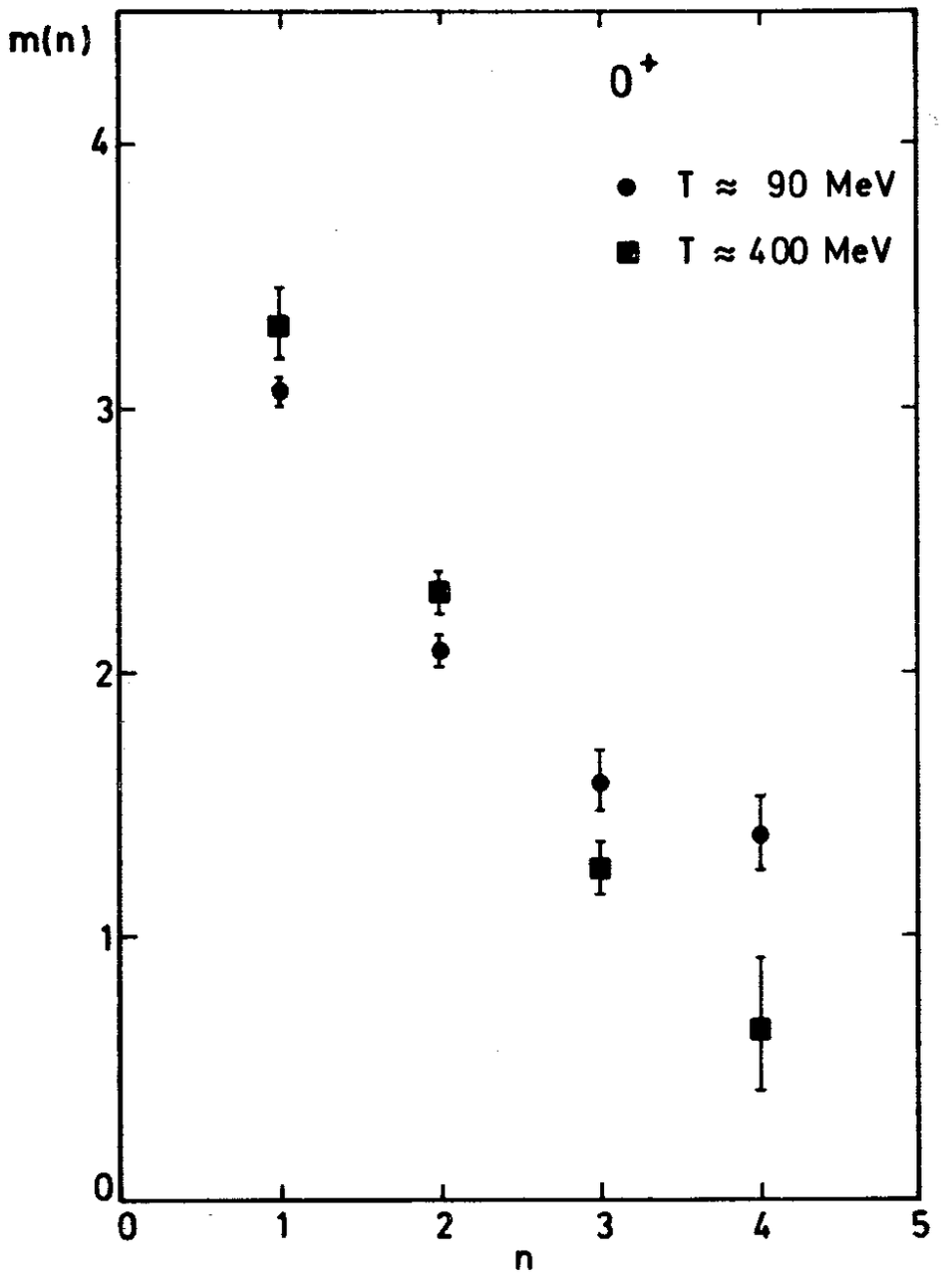

Fig 24

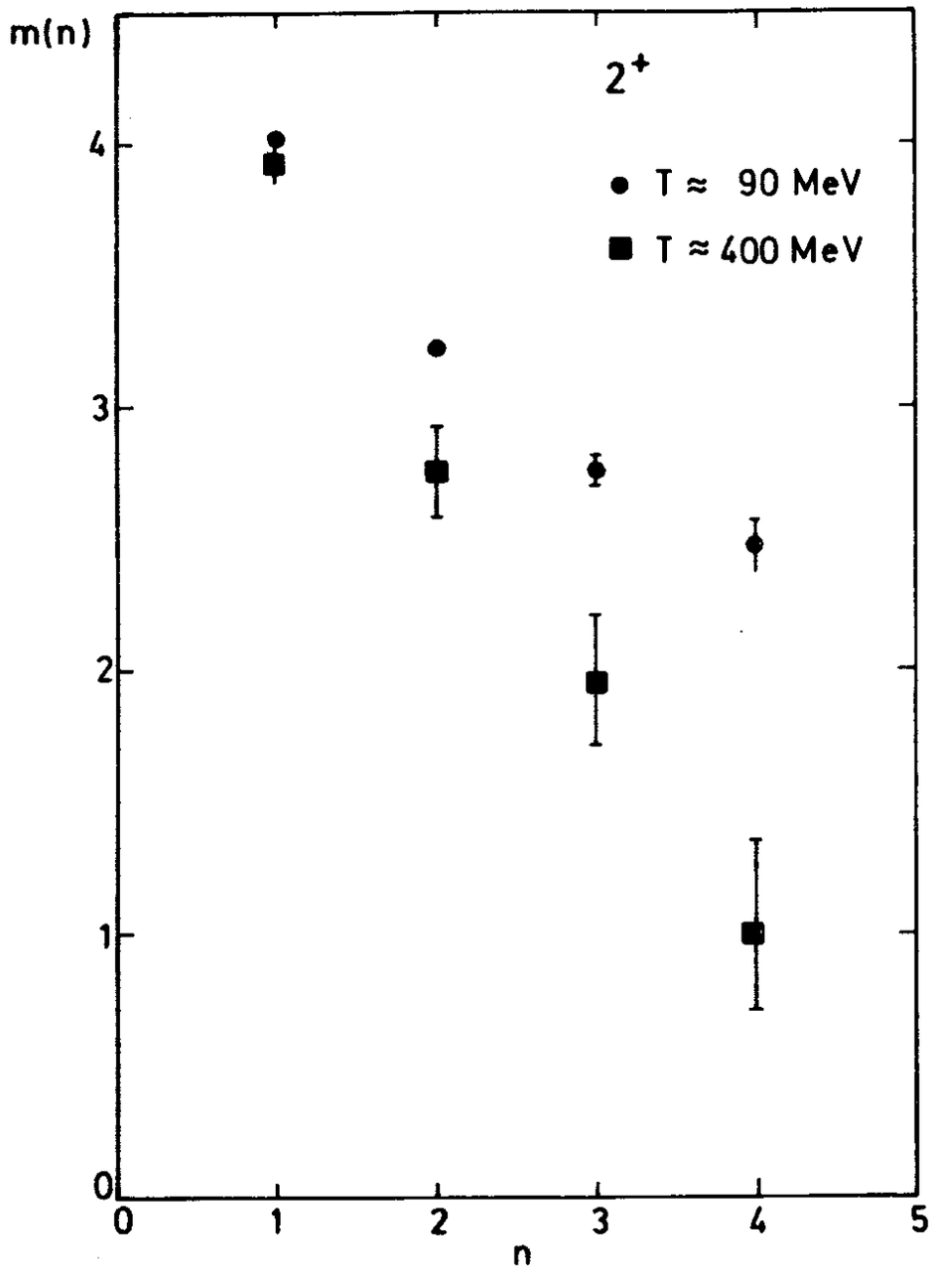

Fig 25